nature communications



Article

https://doi.org/10.1038/s41467-024-51582-5

Replay-triggered brain-wide activation in humans

Received: 22 September 2023

Accepted: 8 August 2024

Published online: 21 August 2024



Qi Huang^{1,2,8}, Zhibing Xiao ^{1,2,8}, Qianqian Yu^{3,8}, Yuejia Luo^{1,3,8}, Jiahua Xu², Yukun Qu^{1,2}, Raymond Dolan ^{1,4,5}, Timothy Behrens^{5,6,7} & Yunzhe Liu ^{1,2}⊠

The consolidation of discrete experiences into a coherent narrative shapes the cognitive map, providing structured mental representations of our experiences. In this process, past memories are reactivated and replayed in sequence, fostering hippocampal-cortical dialogue. However, brain-wide engagement coinciding with sequential reactivation (or replay) of memories remains largely unexplored. In this study, employing simultaneous EEG-fMRI, we capture both the spatial and temporal dynamics of memory replay. We find that during mental simulation, past memories are replayed in fast sequences as detected via EEG. These transient replay events are associated with heightened fMRI activity in the hippocampus and medial prefrontal cortex. Replay occurrence strengthens functional connectivity between the hippocampus and the default mode network, a set of brain regions key to representing the cognitive map. On the other hand, when subjects are at rest following learning, memory reactivation of task-related items is stronger than that of pre-learning rest, and is also associated with heightened hippocampal activation and augmented hippocampal connectivity to the entorhinal cortex. Together, our findings highlight a distributed, brain-wide engagement associated with transient memory reactivation and its sequential replay.

Imagine tackling a complex puzzle, and then, during moments of rest, your brain spontaneously begins to piece together the solution. This process mirrors a neural phenomenon known as 'replay', characterized by the fast reactivation of experiences in sequence^{1,2}. A replay sequence may repeat past experiences, but may also predict the future^{3,4}, or even reorganize experiences for flexible behavior⁵⁻⁷, such as solving a complex puzzle⁸. Replay is also thought to promote hippocampal-cortical dialogue in general⁹⁻¹², but its exact spatial and temporal dynamics are unclear.

Replay, first identified in the rodent hippocampus during sleep^{1,2}, has subsequently been observed during wakeful rest and while on-task, and is now considered to serve a broad spectrum of cognitive functions^{13,14}. Initial studies suggested that replay (during sleep) plays a

crucial role in consolidating past experiences⁹⁻¹². Further research has extended the recognized functions of replay beyond mere memory consolidation¹³. Replay assists in reorganizing experiences, for instance, by spontaneously representing rules or identifying shortcuts in a maze⁵⁻⁷. It supports reminiscing about past experiences^{6,15,16}, understanding the present^{5,17}, and planning for the future^{3,4}. Consequently, replay has been detected not only in the hippocampus but in other brain regions as well¹⁸, including the visual cortex¹⁹ and entorhinal cortex (EC)²⁰. These replays occur either in coordination with, or independently from, hippocampal replay. However, the restricted spatial coverage of invasive neural recordings means that the comprehensive pattern of whole-brain activation associated with replay events remains largely uncharted.

¹State Key Laboratory of Cognitive Neuroscience and Learning, IDG/McGovern Institute for Brain Research, Beijing Normal University, Beijing, China. ²Chinese Institute for Brain Research, Beijing, China. ³School of Psychology, Center for Brain Disorders and Cognitive Science, Shenzhen University, Shenzhen, China. ⁴Max Planck University College London Centre for Computational Psychiatry and Ageing Research, London, UK. ⁵Wellcome Centre for Human Neuroimaging, UCL, London, UK. ⁶Wellcome Centre for Integrative Neuroimaging, University of Oxford, Oxford, UK. ⁷Sainsbury Wellcome Centre for Neural Circuits and Behaviour, UCL, London, UK. ⁸These authors contributed equally: Qi Huang, Zhibing Xiao, Qianqian Yu, Yuejia Luo. — e-mail: yunzhe.liu@bnu.edu.cn

In humans, noninvasive neuroimaging has found evidence for memory reactivation^{21–23} and more recently, sequential replay^{6,24}, findings that align with those observed in rodent studies²⁵. During planning, Kurth-Nelson, et al ²⁶ reported fast neural sequences with a transition speed of 40 ms lag using Magnetoencephalography (MEG). The time compression seen in these sequences resembled those observed in rodent replay^{10,12}. During rest, reverse replay of past experiences, has been selectively linked to value learning. This was identified using both MEG^{3,6} and Electroencephalography (EEG)²⁷, a finding consistent with the animal literature¹⁶. While M/EEG provides valuable insights into the rapid dynamics of replay, it does not offer precise information about the source of replay signals.

Human functional magnetic resonance imaging (fMRI) has been used to localize sequential neural replay to specific brain regions^{24,28,29}. Wittkuhn and Schuck²⁸, employed fMRI to index the sequence of predictive probabilities within a time repetition (TR), reporting on-task sub-second activations of visual stimuli in the occipital-temporal cortex. During rest, Schuck and Niv²⁴ reported positive correlation between the frequencies of transitions between decoded states and the expected distances between these states in the hippocampus. However, fMRI is limited in its ability to discern the directionality and speed of replay²⁸, characteristics that are likely important given that previous human M/EEG studies^{3,6,30,31}, as well as animal research^{24,28,29}, have shown a correspondence to different functional aspects of replay. To date, no study has been able to simultaneously record replay events and capture high spatial resolution, whole-brain activity in humans (cf. related work by Higgins, et al.³² on MEG source localization).

While replay is thought to be related to a variety of cognitive functions, it is useful to consider these as broadly serving two general aspects: the offline formation of a cognitive map during rest and sleep, and the on-task utilization of this map for guiding behaviour²⁵. Here, a 'cognitive map' is used in its most general sense, referring to a structured mental representation of experiences, without distinguishing between narrative or schema^{17,33,34}. Understanding the dynamics of replay in relation to broader brain activation is crucial, especially the role of the default mode network (DMN). The DMN, a set of brain regions, shows increased activity during rest³⁵ or internal cognition tasks, such as mental simulation or imagination³⁶, and is hypothesized

to encode our world knowledge, or cognitive map^{37–39}. However, the interplay between replay dynamics and the DMN during both task and rest remains underexplored. This is due to the temporal transience of hippocampal replay and the spatial distribution of the DMN, with neither M/EEG nor fMRI alone being sufficient to capture these neural processes simultaneously.

In the current study, we examine memory reactivation of task-related items and their sequential replay during mental simulation and wakeful rest. Task-related reactivation refers to the spontaneous reactivation of past experiences, recognized through decoding models, while sequential replay is defined as the sequential reactivation of those experiences. The simultaneous use of EEG-fMRI recording offers a unique opportunity to explore these phenomena in greater depth⁴⁰⁻⁴². The fine temporal resolution of EEG captures fast neural replay and provides timestamps of replay events, enabling the probing of brain-wide activation with fMRI. We focus on the whole-brain activation and the hippocampal functional connectivity to other brain regions at the times of transient replay events, both during rest and while on-task.

Results

Task and analysis pipeline

With simultaneous EEG-fMRI recordings, subjects were tasked with mentally connecting dots that were separate in experience but could be linked together based on a learnt relational structure. This cognitive map is a one-dimensional line. Previous studies have shown that a similar task, with two sequences (comprised of six pairwise associations), elicits offline reactivations during rest, which can be detected using either MEG⁶ or EEG²⁷. The current task is modified to include a directional cue to test if replay directionality during mental simulation is subject to explicit instruction. The task is also simplified to contain only one sequence of four objects.

The task starts with a functional localizer session (Fig. 1), used to train decoders, during which subjects were presented with one of four images. They were encouraged to think about the image's semantic content and were later asked to determine whether the following text matched the preceding image. As in previous studies, subjects were unaware of task-related information during the functional localizer

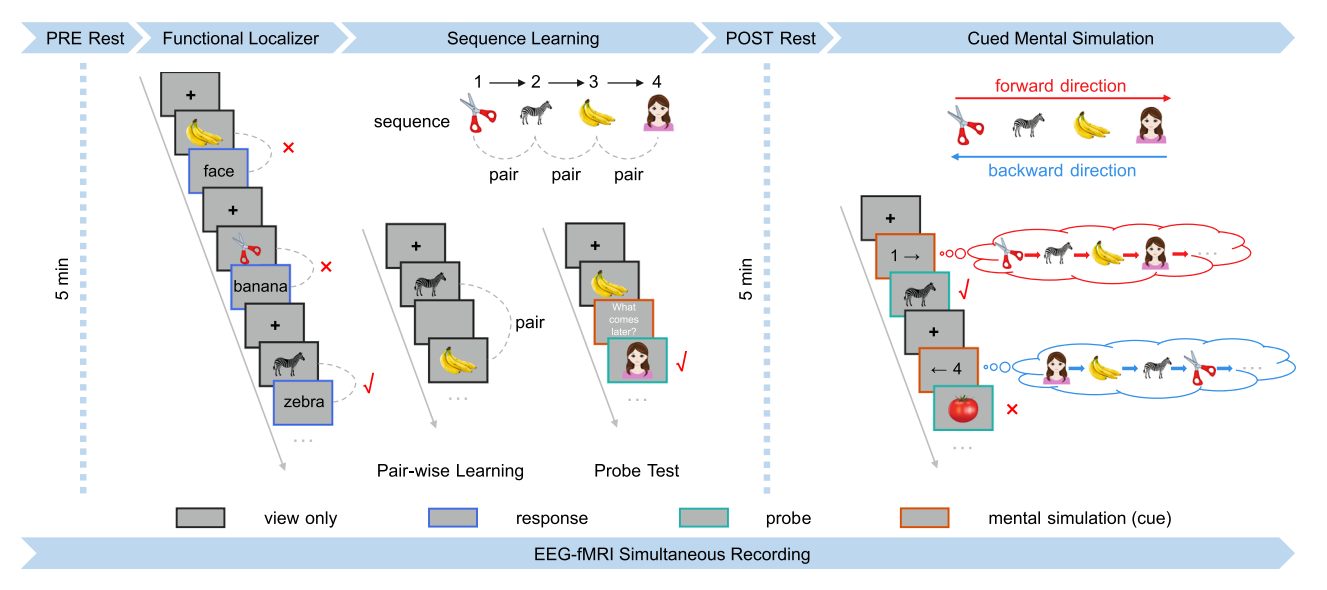


Fig. 1 | Experimental design of a cued sequential mental simulation task with simultaneous EEG-fMRI. Subjects, undergoing simultaneous EEG-fMRI recordings, were required to construct a sequence by learning pairwise associations of four discrete visual stimuli. They were then cued to mentally simulate the learned sequence in either a forward or reverse order. As in previous replay

studies^{3,6,30,32,45,46}, stimuli were first presented in a random order during functional localizer phase, prior to learning. We included a resting state both before (PRE Rest) and after learning (POST Rest) and this allowed us to measure changes in spontaneous neural activity induced by learning.

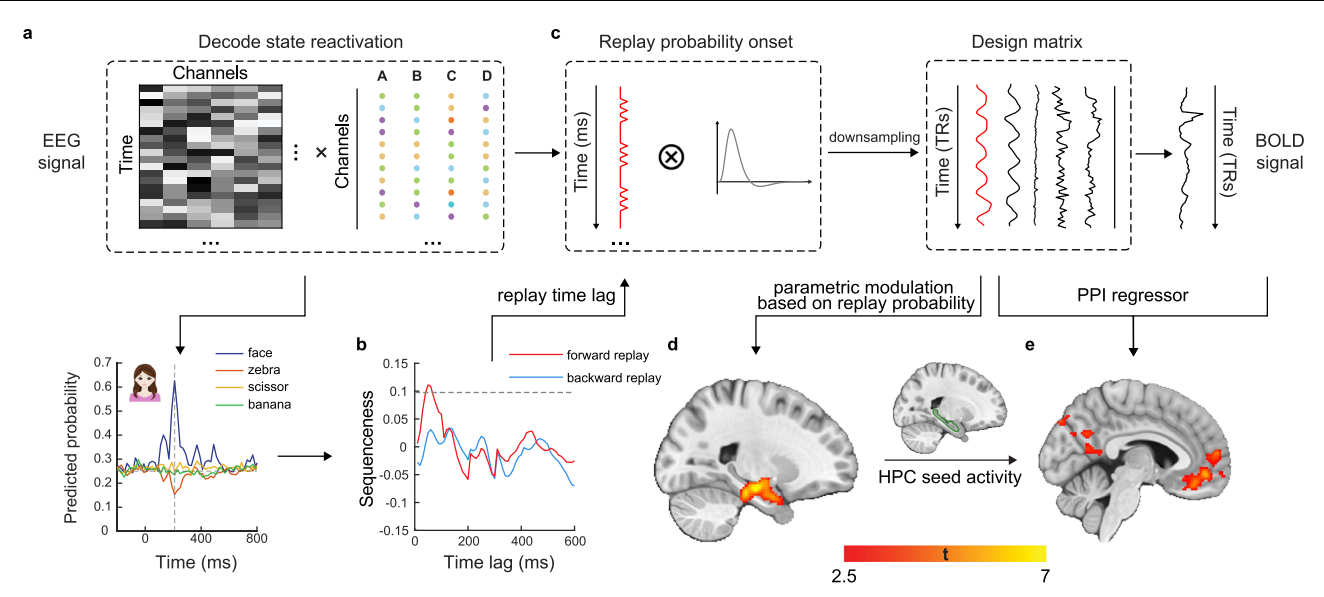


Fig. 2 | **Simultaneous EEG-fMRI analysis framework for studying sequential replay. a** EEG-based stimuli classifiers were trained using whole-brain channel features during the functional localizer and later used to decode stimuli reactivations during specific task phases, such as rest or during mental simulation. **b** Temporal Delayed Linear Modelling (TDLM) was applied to the decoded time series to measure the sequential reactivation of states (e.g., visual stimuli) separately for forward and reverse order⁴³. **c** After identifying a time lag of interest (e.g., the peak of sequenceness), we derived an EEG-based replay probability time course. This was then convolved with the hemodynamic response function (HRF) and

down-sampled to match the fMRI time resolution, serving as an additional regressor in an fMRI-based GLM analysis. ${\bf d}$ Based on the new GLM, we determined when (via EEG) and where (via fMRI) replay occurs. ${\bf e}$ Using an fMRI-derived ROI (green trace, hippocampus), this EEG-based replay probability can be used (by multiplying with ROI neural activity) to detect changes in functional connectivity with other brain regions as a function of replay probability (i.e., psychophysiological interaction, PPI). Data shown here (decoding, EEG replay and coupled fMRI pattern) are from representative subjects. Results are presented with $P_{unc.}$ < 0.01 for illustrative purpose and reported using the MNI coordinate system.

session. This session was used to train decoders for both EEG²⁷ and fMRI signals²⁸. After this, three pairwise associations were presented in a randomized order (e.g., $1 \rightarrow 2$, $3 \rightarrow 4$, $2 \rightarrow 3$), and subjects were required to mentally link the associations into a sequence (i.e., $1 \rightarrow 2 \rightarrow 3 \rightarrow 4$), a process we term sequence learning. Only those subjects who achieved at least 90% accuracy in the last learning run proceeded to the cued mental simulation task. A resting state period was included both before (PRE Rest) and after learning (POST Rest). After that, subjects were asked to mentally simulate the sequence in either a forward or reverse order, based on the cue ($1 \rightarrow$, forward; $\leftarrow 4$, backward). Our subsequent analyses included 33 subjects who completed all task sessions with simultaneous EEG-fMRI recording.

Utilizing the fine spatiotemporal resolution offered by simultaneous EEG-fMRI, our goal is to determine when and where neural replay occurs in the brain. This involves indexing fast replay events through EEG and imaging replay-aligned brain-wide activation in fMRI. In brief, our analysis pipeline comprises five steps (Fig. 2). First, we train neural decoding models for each image based on EEG data from the functional localizer session. These models are then applied to decode their neural reactivations during mental simulation and offline resting time. After decoding, we quantify the strength of sequential reactivations (or replay) in a sequence (e.g., $1 \rightarrow 2 \rightarrow 3 \rightarrow 4$), separately for forward and reverse order⁴³. If there is significant evidence for replay, we can calculate when such replay occurs and the strength of this evidence. To model this replay probability in fMRI, we convolve it with a canonical hemodynamic response function (HRF), and down-sample it to match the temporal resolution of the fMRI signal. Replay probability can then be encoded as an additional psychological condition using a general linear model (GLM) in fMRI. In addition to localizing replay, we can model its psychophysiological interaction (PPI)⁴⁴ to explore how functional connectivity between a region of interest (ROI, e.g., the hippocampus) and other brain regions changes as a function of replay probability. Notably, this analysis pipeline is not restricted to replay; we can investigate the spatiotemporal dynamics of any task reactivations in the same way.

EEG-based and fMRI-based neural decoding

During the functional localizer, subjects were instructed to press key '1' when a text matched the semantic content of its preceding image (congruent condition), and '2' otherwise (incongruent condition). The mean behavioural accuracy was 94.57 ± 0.70%, where chance level is 50%. Following the analysis step outlined above, we trained four separate one-vs-rest logistic regression classifiers based upon EEG data from correct trials, one for each image. As in previous M/EEG-based replay studies^{3,6,26,27,30,32,43,45,46}, we trained EEG decoding models using all available channels as features at a single time bin (10 ms) and tested performance at all time points from 200 ms prior to the stimulus onset to 800 ms post onset (Fig. 3a). The peak cross-validated decoding accuracy was observed at 210 ms post stimulus onset (46.25 ± 0.95%, compared with a chance level of 25%, $t_{(32)} = 22.41$, P < 0.001). To further examine the sensitivity of the classifiers to each image, we analyzed the time course of predicted probability separately for each image (Fig. 3b). All image classifiers showed above-chance probability in predicting the images they were trained on (dark grey lines) and not for other images (lighter grey lines). Based on these results, the image classifiers were trained at 210 ms post stimulus onset for our subsequent EEG-based replay analysis. Note, similar decoding accuracy and temporal dynamics were observed in a pilot subject who performed under both standalone EEG and simultaneous EEG-fMRI settings, indicating consistent neural dynamics across both settings (Supplementary Fig. 1a).

Contrary to the fine temporal resolution offered by EEG, fMRI is better suited for localizing where in the brain a specific cognitive process unfolds. In fMRI, we found significant activation in the visual cortex when an image was on-screen, with also class-specific activation patterns observed (Supplementary Fig. 2a). Moreover, heightened activation was detected in the temporal cortex and anterior cingulate

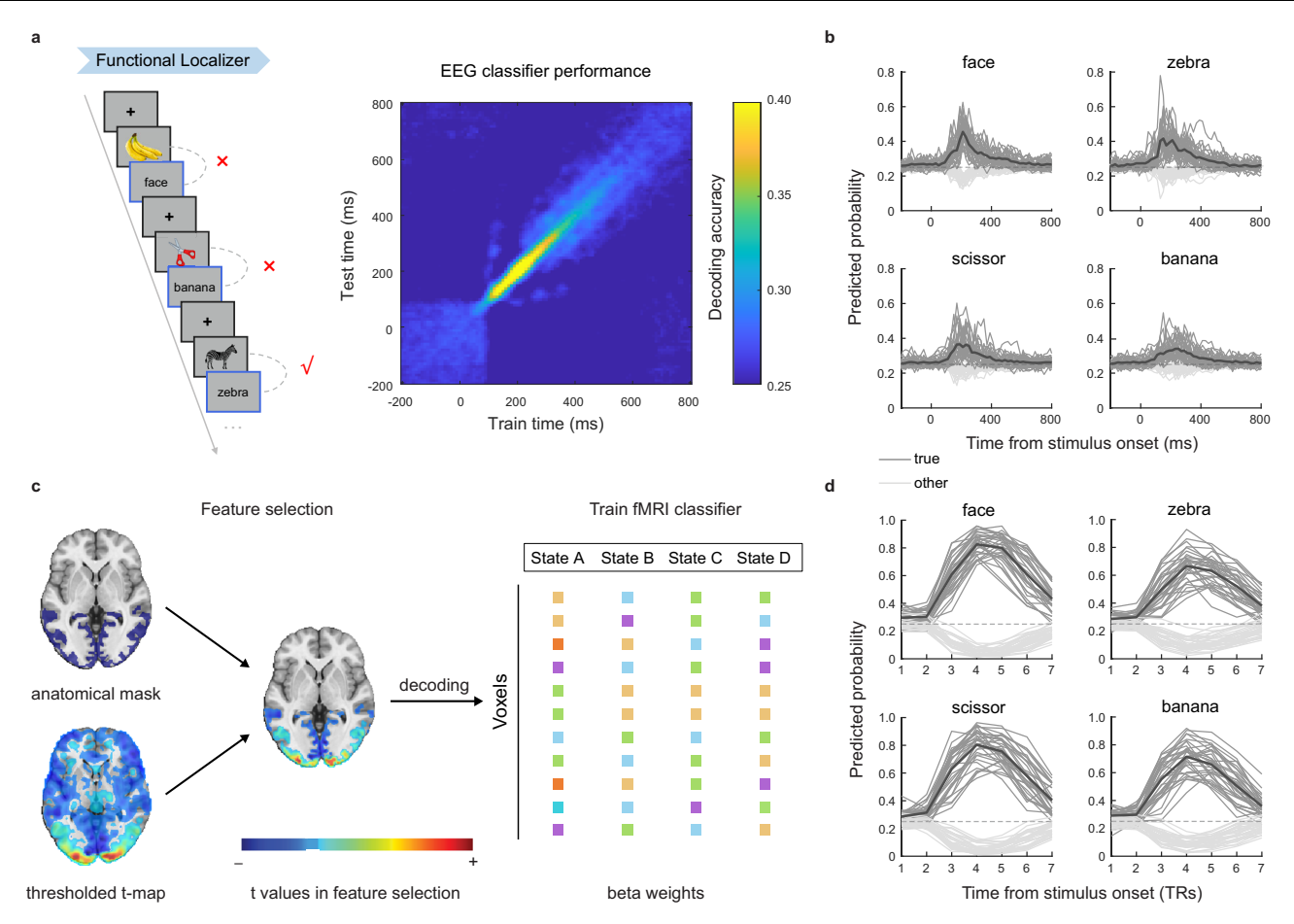


Fig. 3 | **EEG-based and fMRI-based decoding during functional localizer. a** The mean cross validated decoding accuracy of EEG-based classifiers. As in previous studies 3,6,27,30,32,45,46 , classifiers were trained independently at each time point and tested on all time points, starting from 200 ms before stimulus onset to 800 ms post onset (10 ms time bin) during the functional localizer task (left panel). Decoding accuracy peaked at 210 ms post-stimulus onset. n = 33. **b** The time course (-200 - 800 ms) of mean EEG-based decoding probability trained and tested at the same post-stimulus onset (black line), separately for each stimulus. The dark grey lines represent the decoding probability of a particular classifier for a given image (black line represent the mean probability across subjects), while the light grey lines represent the mean decoding probability of the same classifier for other images.

n=33. **c** Feature selection procedure in fMRI-based decoding. Following Wittkuhn and Schuck²⁸, we selected the subject-specific anatomical masks combined with thresholding t-maps (t> 3) to identify voxels that selectively response to functional localizer. Note that the result presented here was selected from a representative subject for illustrative purpose only. **d** The time course (in TR, starting from stimulus onset) of mean fMRI-based decoding probability trained and tested at the same post-stimulus time, separately for each stimulus. The dark grey lines represent the decoding probability of a particular classifier for a given image (black line represent the mean probability across subjects), while light grey lines represent the mean decoding probability of the same classifier for other images. n = 33. Source data are provided as a Source Data file.

cortex (ACC) when semantic text was presented (Supplementary Fig. 2b). We decoded images from the fMRI signal as in Wittkuhn and Schuck²⁸. We first performed feature selection based on anatomical mask and functional t map (Fig. 3c), and found a peak cross-validated decoding accuracy of $83.39 \pm 1.77\%$ (compared with a chance level of 25%, $t_{(32)} = 38.00$, P < 0.001), at the 4^{th} TR post stimulus onset (Fig. 3d), consistent with Wittkuhn and Schuck²⁸.

In both EEG and fMRI-based decoding, the predicted probability for the true stimulus significantly exceeded the chance level (25%, EEG: all $t_{(32)} \ge 8.47$, P < 0.001; fMRI: all $t_{(32)} \ge 20.63$, P < 0.001, Fig. 3b & d). A key advantage of simultaneous EEG-fMRI recording is its capability to examine activations in response to the same event. We observed a significant positive correlation across subjects between the decoding accuracies of EEG and fMRI classifiers (robust correlation, r = 0.49, P = 0.004, see Supplementary Fig. 1c), consistent with them capturing the same cognitive processes.

Spatiotemporal dynamics of neural replay during mental simulation

Human replays have been found to spontaneously reorganize experience in a manner that corresponds to a learnt relational

structure^{3,6,26,27,30,32,45,46}. In a sequence learning session, subjects learnt to form a linear sequence consisting of four images based on three pairwise associations experienced in randomized order. During learning, images from pairwise associations were presented serially with heightened activation in visual cortex, dorsal lateral prefrontal cortex (DLPFC) and hippocampus was evident at the onset of the 1st compared to the 2nd image (Supplementary Fig. 3a). Over the course of learning, hippocampal engagement by the 2nd image increased $(\beta = 0.015 \pm 0.005, P < 0.001,$ Supplementary Fig. 3b), consistent with its role in associative learning 38,47. Behavioral performance significantly increased with learning experience ($F_{(32)} = 19.04$, P < 0.001), aligning with heightened hippocampal activity observed in the second item over trials. During the probe phase, a target image was first presented on the screen, then subjects were asked to think of which image comes next. A probe image was then shown, and subjects were required to determine if it was correct or not. We found significant activation in the ACC, DLPFC and insular cortex at the onset of the target image (Supplementary Fig. 3c), and higher ACC activation to the probe image for correct vs. error response trials (Supplementary Fig. 3d). Across all subjects, the mean accuracy of the probe test was 93.86 ± 1.20%, indicating successful learning of the sequence. The mean accuracy of

the last run was $99.49 \pm 0.35\%$ across subjects; no subjects were excluded from the analysis based on the criterion of > 90% accuracy.

After sequence learning, subjects were instructed to mentally simulate the sequence in either forward or reverse order based on a given cue. Subsequently, they were required to identify whether a probe image was part of the sequence. The average behavioral accuracy was $93.59 \pm 0.82\%$. Subjects were also asked to rate the vividness of their subjective experience on a scale from 1 to 4. All participants reported a high level of vividness with a mean rating of 3.35 ± 0.07 . No significant difference was found between forward and backward mental simulation in terms of behavioral accuracy ($t_{(32)} = -0.98$, P = 0.335) or vividness rating ($t_{(32)} = 1.50$, P = 0.143).

At the beginning of each simulation trial, a directional cue, " $1 \rightarrow$ " or " \leftarrow 4" appeared. If replay can be modulated by explicit instruction, we would predict a shift in the direction of replay (if it exists) that aligns with the cued instruction. By contrast, if replay corresponds to a more unconscious and spontaneous process, then we would expect the direction of replay to be independent of the cue.

In the human neuroimaging literature to date, there are two ways to quantify task-related sequential reactivations or replay during task. One is Temporal Delayed Linear Modelling (TDLM)⁴³, which calculates the mean sequenceness over all time bins, independently at different speeds (time lags), separately for forward and reverse direction. This method is mainly used in M/EEG studies^{3,6,27,30,32,45,46} but can, in principle, be applied to fMRI data⁴³. The second method uses fMRI data²⁸, and calculates the regression slope that predicts the position of a state based on the rank of the state probability at each time bin (or TR in fMRI terminology). Figure 4a, provides an illustration separately for the TDLM method and fMRI-based regression method. In addition, another method for detecting fMRI-based off-task replay is from Schuck and Niv²⁴, calculates the similarity between an hypothesized transition matrix (state distances) and an empirical transition matrix (transition frequency between states) within a brain region of interest (ROI) during rest. In principle, this method can also be applied to the cued mental simulation session.

Using TDLM on the EEG-based decoding, we indeed found selective significant forward replay from 30 to 50 ms time lag in cue "1 \rightarrow " trials (peak at 30 ms lag, β = 0.021 \pm 0.012, Fig. 4b upper panel), as well as forward replay from 20 to 40 ms time lag in cue " \leftarrow 4" trials (peak at 30 ms lag, β = 0.023 \pm 0.012, Fig. 4b bottom panel). As the subjects' task experience increased, their replay strength during mental simulation increased ($t_{(32)}$ = 4.18, P < 0.001). However, vividness ratings of this simulation, elicited as a subjective measure, were found uncorrelated with replay strength ($t_{(31)}$ = -0.55, P = 0.585). Extending the time lag scale to 2000 ms, to identify replay events at longer timescales, failed to reveal additional replay events (either forward or backward) beyond those detected at a peak of 30 ms (see Supplementary Fig. 4).

In fMRI-based decoding, we also applied TDLM method to the fMRI-based data. While there was a suggestion of replay in some individuals, no significant fMRI-based replays were found across subjects (Supplementary Fig. 5). Likewise, using the regression method²⁸, we did not observe any significant regression slope in either time bin or condition (all $P_{corr.} \ge 0.06$, two-sided one-sample t-test against zero, Fig. 4c), nor was there any significant difference between the 1st and 2nd periods (forward: $t_{(32)} = 1.14$, P = 0.260; backward: $t_{(32)} = -0.175$, P = 0.862, two-sided paired t-test, Fig. 4c). Similarly, applying the method from Schuck and Niv²⁴ obtained non-significant fMRI-based replay (Supplementary Fig. 6a-b).

To determine where in the brain on-task neural replay occurs, we identified putative replay events at 30 ms time lag and modelled these in a GLM to predict the fMRI signal. After convolving replay events with the HRF and down-sampling, the replay probability time series was modelled as a parametric modulator of the 10 s mental simulation regressor. We found that the occurrence of replay was associated with activations in both the hippocampus and medial prefrontal cortex

(mPFC, Fig. 4d, see also Supplementary Fig. 7a for activations of the mental simulation regressor). This result is consistent with previous findings on MEG replay source localization^{3,6,30,31,45}, suggesting that human replay, as is the case in rodents^{11,48,49}, originates from hippocampus. We also explored brain-wide activation related to single-item reactivation and found increased activity in both the hippocampus and mPFC (see Supplementary Fig. 7b), the same regions that exhibited higher activation in relation to sequence replay events.

We next investigated how functional connectivity between the hippocampus and other brain regions (e.g., DMN) changes in relation to variations in replay probability⁴⁴. As replay probability increased, there was a significant increase in hippocampal-seed connectivity with DMN, including the mPFC⁵⁰⁻⁵⁴, and the posterior cingulate cortex (PCC)^{53,55}, as well as the visual cortex^{56,57} (see Fig. 4e). We also explored changes in mPFC-based functional connectivity as a function of replay probability. This revealed significant increases in connectivity between the mPFC-seed and other DMN regions, including the PCC and angular gyrus, as well as with the visual cortex, but not with the hippocampus (see Supplementary Fig. 7c-d). These results are consistent with a flow of replay information from the hippocampus to the mPFC, and subsequently to other DMN regions and the visual cortex. However, we acknowledge that PPI analyses do not allow for causal or directional inference.

Spatiotemporal dynamics of learning-induced task reactivation during rest

The findings detailed above indicate that simultaneous EEG-fMRI can index when and where of on-task replay. We next applied this analysis pipeline to rest periods, where, unlike task data, there are no obvious timestamps for specific cognitive processes. Nevertheless, identifying spontaneous reactivation or replay during rest can provide naturalistic timing information for modelling resting-state activity²⁵. We assumed the absence of significant task-related replay during the PRE Rest period, given subjects had not yet experienced the visual stimuli or acquired any structural knowledge. In contrast, during the POST Rest period, after sequence learning, we predicted the presense of replay⁶. However, our TDLM analysis did not find evidence of replay in either EEG or fMRI-based decoding during the PRE or POST Rest period (Supplementary Fig. 8). Similarly, using Schuck and Niv²⁴ method to detect replay using fMRI, we found no significant evidence of replay in either the PRE or POST Rest period (see Supplementary Fig. 6c).

The relatively simple sequence setup in the current study, which only involved one sequence as opposed to two sequences used in Liu, et al.⁶, might entail less of a need for sequential replay during rest^{3,58,59}. Next, we analyzed the mean reactivation strength of task-related stimuli, without requiring them to be in sequence. Mean reactivation probabilities were calculated by averaging across all time points and all task stimuli during each rest period. We found that the mean reactivation strength of stimuli, regardless of their sequential order, was significantly higher in the POST Rest compared to the PRE Rest period $(t_{(31)} = 2.75, P = 0.010, \text{ two-sided paired } t\text{-test}; \text{ Fig. 5a})$, suggesting enhanced task reactivations following learning.

We did not find significant correlations between single-item reactivation strength during POST rest and any behavioural performance measures. This includes sequence learning task performance (r=-0.09, P=0.619), cued mental simulation task performance (r=-0.09, P=0.607), and vividness ratings (r=-0.13, P=0.456). The same was true for PRE rest (all r<0.15, P>0.5). These null results may be due to a ceiling effect and limited variability in behavioural performance. Participants consistently demonstrated high accuracy in the last run of the sequence learning task $(99.49\pm0.35\%)$, overall sequence learning $(93.86\pm1.20\%)$, cued mental simulation $(93.59\pm0.82\%)$, and vividness ratings (3.35 ± 0.07) .

To explore offline reactivation-triggered whole-brain activity patterns, we applied our analysis pipeline to task-related reactivation

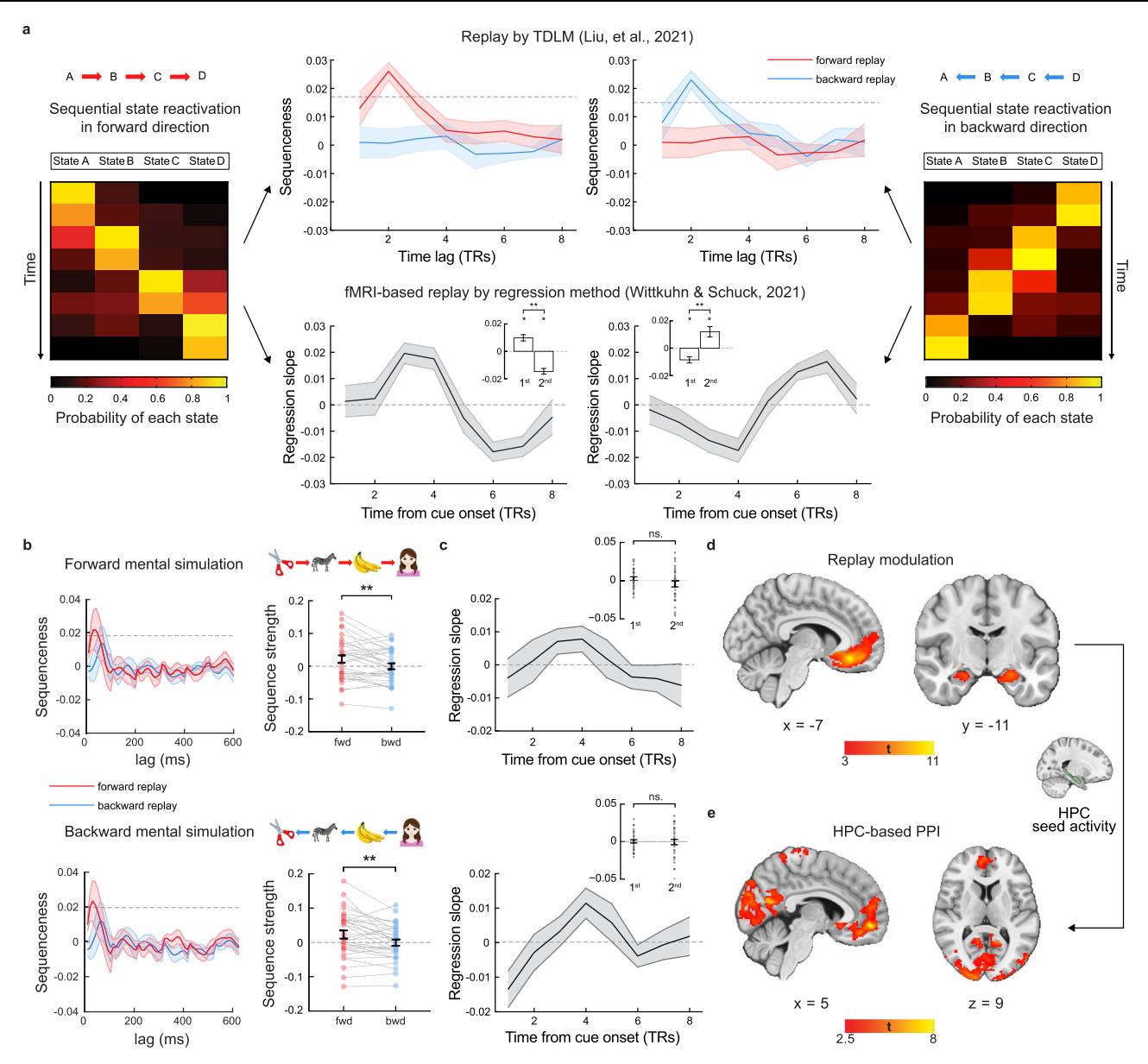


Fig. 4 | EEG-based and fMRI-based replay during cued mental simulation, a The illustration of two analysis methods for detecting replays. TDLM⁴³ is used primarily with MEG^{3,6,30,32,45,46}, and more recently also with EEG²⁷. The other is a regression method, as per Wittkuhn and Schuck²⁸ and primarily used with fMRI²⁹. Please note that this panel is solely for illustrative purposes. For results based on actual data, refer to Supplementary Fig. 5 and Panel c. **b** EEG-based replay with TDLM, separately for forward (cued " $1 \rightarrow$ ", top row) and backward (cued " $\leftarrow 4$ ", bottom row) mental simulation conditions. There were significant forward (but not reverse) replays during both forward and backward mental simulation. Sequence strength on the peak time lag (30 ms) is shown on the right, separately for forward and backward mental simulation conditions (two-sided paired t-test, forward condition: $t_{(32)} = 2.80$, P = 0.009; backward condition: $t_{(32)} = 3.09$, P = 0.004). The grey dash line represents the permutation threshold, defined as the 95th percentile of the permutated transitions of interest controlling for multiple comparisons. n = 33. c fMRI-based neural sequence with regression method28, separately for forward and backward mental simulation conditions. There was no significant evidence for sequential activation in the correct order (all $P_{\text{corr.}} \ge 0.06$, two-sided one-sample ttest against zero, FDR corrected). The bar plot in the upper right corner shows

mean slope coefficients for each period (two-sided paired t-test, forward condition: $t_{(32)} = 1.14$, P = 0.260; backward condition: $t_{(32)} = -0.175$, P = 0.862). None of these coefficients were significantly different compared to zero. See Supplementary Fig. 5 for assessing fMRI replay using TDLM, as well as results from single subject for illustration purpose. n = 33. **d** The parametric modulation of EEG-based replay probability in the whole-brain fMRI during mental simulation showed significant activations in hippocampus and mPFC. We use whole-brain FWE correction at the cluster level (P < 0.05) with a cluster-inducing voxel threshold of $P_{unc.} < 0.001$. **e** The psychophysiological interaction (PPI) between hippocampal activity (anatomically defined) and EEG-based replay probability revealed significant functional connectivity change in mPFC, PCC and visual cortex. See Supplementary Fig. 7c-d for mPFC-based PPI results. We use whole-brain FWE correction at the cluster level (P < 0.05) with a cluster-inducing voxel threshold of $P_{unc.} < 0.01$. Each dot is one subject. The grey lines connect results from the same subject. Shaded areas in **b** and c show SEM across subjects. Error bars in b and c show SEM across subjects. * P < 0.05, ** P < 0.01, ns., not significant. Abbreviation: HPC - hippocampus. Source data are provided as a Source Data file.

during rest by summarizing the EEG-based reactivation across stimuli. These reactivation events were then convolved with the HRF, and the ensuing reactivation time series was used as a regressor to explain resting-state fMRI signals. We found that higher reactivation strength

correlated with increased hippocampal activation during POST Rest (Fig. 5b; hippocampal ROI analysis, $t_{(32)} = 3.83$, $P_{corr.} < 0.001$, two-sided one-sample t-test), while no activation was identified during PRE Rest, at either the whole-brain or the hippocampal ROI level ($t_{(32)} = 1.08$,

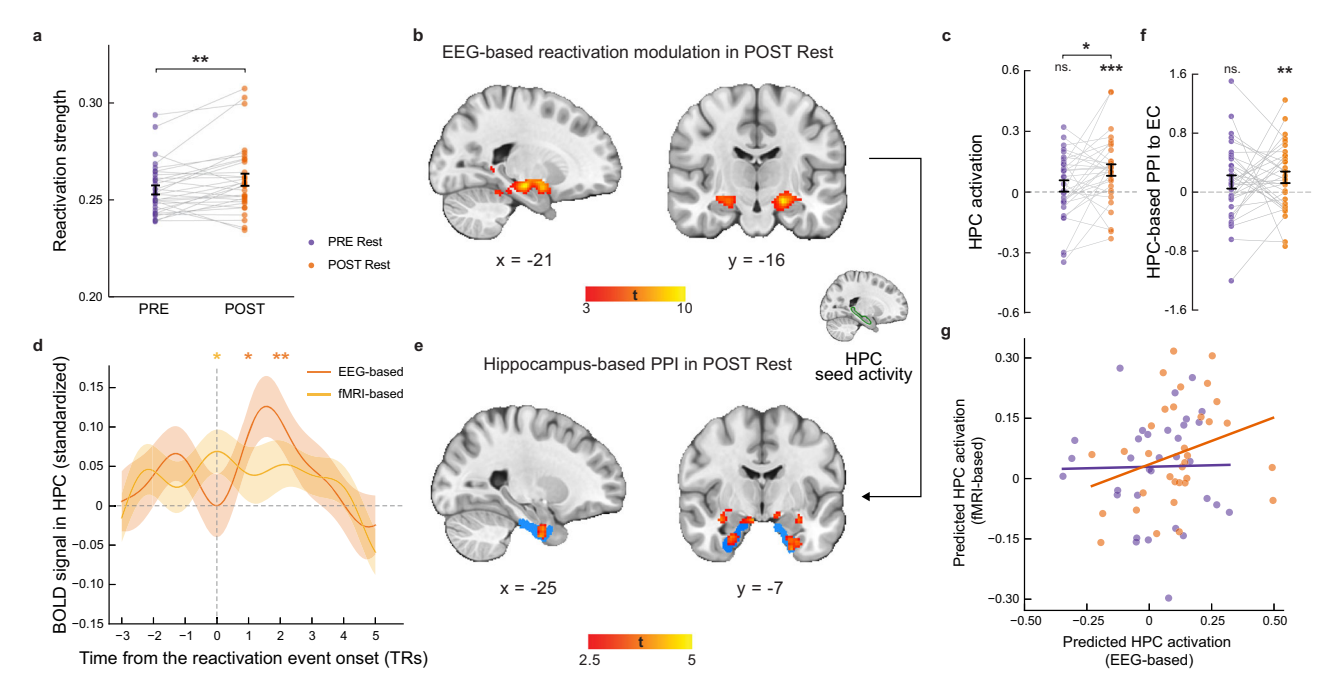


Fig. 5 | EEG-based reactivation during PRE and POST Rest. a In EEG-based task reactivations, there was a significant higher reactivation strength during POST than PRE Rest (two-sided paired t-test: $t_{(31)} = 2.75$, P = 0.010). n = 32, excluding an outlier (beyond three deviation of the mean). **b** Parametric modulation of EEG-based reactivation probability in whole-brain fMRI during POST Rest showed significant activations in bilateral anterior hippocampus (whole-brain FWF correction at the cluster level (P < 0.05) with a cluster-forming voxel threshold of $P_{unc} < 0.001$). c ROI analysis. The EEG-based reactivation explained hippocampal activation (anatomically defined) during POST Rest, and it was stronger from PRE to POST Rest in hippocampus (two-sided one-sample *t*-test: PRE: $t_{(32)}$ = 1.08, $P_{corr.}$ = 0.287; POST: $t_{(32)} = 3.83$, $P_{corr.} < 0.001$; two-sided paired t-test: POST vs. PRE: $t_{(32)} = 2.44$, $P_{corr} = 0.030$; FDR corrected). n = 33 **d**, The task reactivation-aligned BOLD signal in hippocampus during POST Rest. Upon alignment to the onsets of task-related reactivation, we observed a significant increase in hippocampal BOLD activity, peaking at the 2nd TR post-EEG-based reactivation (two-sided one-sample t-test: TR = 1: $t_{(32)}$ = 2.57, P = 0.015; TR = 2: $t_{(32)}$ = 3.02, P = 0.005), and also found at onset of

fMRI-based reactivation (TR = 0: two-sided one-sample t-test: $t_{(32)} = 2.45$, P = 0.020). n = 33. e The PPI between hippocampal activity (anatomically defined) and EEGbased reactivation probability showed increased functional connectivity with EC (anatomical mask depicted in blue) during POST Rest. We thresholded at $P_{unc.}$ < 0.01, K > 10 for visualization. **f** ROI analysis. The PPI revealed a significant increase in hippocampal-seed connectivity with the EC (anatomically defined) during POST Rest when EEG-based reactivation increased. (two-sided one-sample ttest: PRE: $t_{(32)} = 1.48$, P = 0.148; POST: $t_{(32)} = 2.75$, P = 0.010). n = 33. **g** There was a positive correlation between EEG-based and fMRI-based reactivation in explaining hippocampal activity during POST Rest, but not PRE Rest (robust correlation, PRE: r = 0.09, P = 0.602; POST: r = 0.38, P = 0.029), n = 33. The solid lines reflect the robust linear fit. Each dot is one subject. The grey lines connect results from the same subject. Shaded areas in d show SEM across subjects. Error bars in a, c and **f** show SEM across subjects. * P < 0.05, ** P < 0.01, *** P < 0.001, ns., not significant. Abbreviation: HPC - hippocampus. Source data are provided as a Source Data file.

 $P_{corr.}$ = 0.287). Moreover, hippocampal activation was significantly stronger during POST Rest compared to PRE Rest ($t_{(32)}$ = 2.44, $P_{corr.}$ = 0.030, two-sided paired t-test, Fig. 5c). As a control analysis, we found that no EEG-based reactivation explained activity in the primary motor cortex (M1), during either PRE or POST Rest or their differences (all $t_{(32)} \le 1.20$, $P \ge 0.24$).

When we applied the same analysis pipeline to fMRI-based task reactivation, we found no significant increase in reactivation for POST Rest compared to PRE Rest ($t_{(32)} = 0.92$, $P_{corr.} = 0.363$; Supplementary Fig. 9a). However, consistent with EEG-based findings, the strength of fMRI-based reactivation correlated with increased hippocampal activation during POST Rest (see Supplementary Fig. 9b-c; hippocampus ROI analysis: $t_{(32)} = 2.87$, $P_{corr.} = 0.021$), but not during PRE Rest ($t_{(32)} = 1.25$, $t_{corr.} = 0.329$). Interestingly, by aligning to the onset of EEG-based reactivation, a significant increase in hippocampal BOLD activity was observed, peaking at the $t_{corr.} = t_{corr.} = t$

We have also examined functional connectivity between the hippocampus and other brain regions as a function of task reactivation during rest (Fig. 5e). The PPI analysis revealed a significant increase in hippocampal-seed connectivity with EC during POST Rest when EEGbased reactivation increased (ROI analysis, $t_{(32)} = 2.75$, P = 0.010, Fig. 5f), but not during PRE Rest ($t_{(32)} = 1.48$, P = 0.148). No significant results were found when the analysis is done based on fMRI-based reactivation (all $t_{(32)} \le 1.41$, $P \ge 0.17$).

The differences between EEG- and fMRI-based task reactivation raise an intriguing question as to their relationship. While EEG and fMRI-based reactivation time series themselves were not correlated, nor there was a systematic temporal relationship between them either during task or rest (Supplementary Fig. 10), we found a significant positive correlation of predicted hippocampal activity with EEG-based reactivation and that of fMRI during POST Rest (Fig. 5g, robust correlation, r = 0.38, P = 0.029), not PRE Rest (r = 0.09, P = 0.602). This suggests offline task reactivation may align EEG and fMRI-based representation in hippocampus.

Discussion

The simultaneous EEG-fMRI analysis framework offers a powerful method to probe the brain-wide patterns associated with temporally transient events, such as memory reactivation and its sequential replay. During task, we show that this combined pipeline can detect fast replay events, as reflected in EEG signals (with a 30 ms time lag), and localize these to the hippocampus, as revealed by simultaneous fMRI. We found that replay during mental simulation is a spontaneous process, one that operates independent of explicit task instruction. An increase in EEG indexed replay strength was associated not only with significant fMRI activations in hippocampus and mPFC, but also with a

significant increase in hippocampal-seed connectivity with the DMN and visual cortex. During rest, we observed a marked increase in EEG-based task-related reactivation from pre- to post-learning periods. Here, an increase in reactivation strength was associated with a significant increase in hippocampal activation and increased hippocampal-seed connectivity with the EC.

These results align with previous work in humans. The decoding accuracy and dynamics of simultaneous EEG mirrored those observed in the standalone EEG condition (Supplementary Fig. 1a), as well as previous M/EEG decoding findings^{6,27}. In fMRI-based decoding, we followed the methods described by Wittkuhn and Schuck²⁸ and achieved similar decoding performance, albeit not detecting replay events in fMRI. During mental simulation, we found 30-ms-time-lag ontask replay in EEG, a finding in keeping with previously reported human replay speed^{3,6,26,27,46}. We further showed the EEG-based replay was associated with activation of hippocampus and mPFC, revealed by fMRI, a finding consistent with previous fMRI replay findings²⁴ and MEG source localization^{3,6,30,31,46}.

A key advance in our analysis pipeline is its ability to detect brainwide activation in coordination with replay. During mental simulation. we found hippocampal and DMN activation associated with sequence replay, as well as reactivation in general. The hippocampal connectivity with the DMN also increased as a function of replay strength. The DMN is proposed to encode an internal model of the world^{25,34}. When initializing replay, this increase suggests a query from the hippocampus to a putative cognitive map, possibly serving to align experiences into an ordered structure. Here, it is intriguing to note that our results are consistent with findings from Kaplan, et al.60, who combined electrophysiological recordings of the hippocampus with whole-brain fMRI in anesthetized monkeys. They also align with rodent studies where widespread activation of cortical regions in the DMN is associated with the onset of hippocampal SWRs, a biomarker of replay^{61,62}. These findings collectively suggest possible cross-species relationships between hippocampal replay and the DMN.

The direction of replay is found to be independent of explicit instruction. Likewise, there was no significant evidence for replay with time lags exceeding 100 ms, even when extending the analysis to an upper time lag limit of 2000 ms. In previous studies, replay direction was found to change with task demands, such as value learning3,6, probe questions³¹, and decision-making versus preservation³⁰. A common feature of these prior studies is that a shift in replay direction served a specific computational goal. For instance, replay shifted from forward to backward only for a sequence paired with a reward outcome, but not for a neutral sequence⁶, where reverse replay is hypothesized to support credit assignment^{3,63}. In the current study, verbal instruction alone does not entail any computational demand and the instruction-independent replay pattern suggests that on-task replay may in fact be spontaneous, independent of volition, and conscious mental effort. Consistent with this, we also found no correlation between the subjective rating of vividness of mental simulation and replay strength. While it could be a ceiling effect of vividness rating, it is also possible that the content of replay is more at a semantic level where imagery vividness is likely to exert little impact on replay quality64.

During rest, we found that task reactivation associated with increased hippocampal activity in the POST compared to the PRE Rest period, with enhanced hippocampal connectivity to the EC (Fig. 5d-f). The EC is thought to encode task relational structures⁶⁵, a concept supported by the presence of grid cells in animal research⁶⁶ and grid-like coding in human fMRI studies^{37,38}. It is noteworthy that compared to the mental simulation period, cross-regional communication during rest was predominantly confined to functional connectivity between the hippocampus and EC, rather than with the DMN. This suggests that on-task replay and off-task reactivation, manifest different brain dynamics that is suggestive of serving distinct cognitive functions¹⁴. In

the rodent literature, on-task replay is associated with memory retrieval and planning⁴⁹, whereas rest replay or reactivation is more linked to memory consolidation⁹. Although the exact mechanism is unclear, the increased connectivity between the hippocampus and EC during rest reactivation may relate to their coordinated activity. For instance, Ólafsdóttir, et al.⁶⁷ found evidence that coordinated grid and place cell replay during rest in rodents supports memory consolidation. The differing functions of replay and reactivation pose an intriguing question, where recent theoretical work has attempted to provide a unified account⁶³. We anticipate that simultaneous EEG-fMRI will provide a promising tool for testing these theoretical predictions, especially in the context of human studies.

Despite a marked increase in task-related reactivation from the PRE to the POST Rest period, significant sequential reactivation-or replay-during rest remained elusive. A key challenge in detecting replay during rest might be the relatively diminished quality of EEG signals obtained during simultaneous EEG-fMRI recordings. Rest replay tends to manifest as a temporally dispersed signal, occurring in bursts³², in contrast to the temporally localized and robust signals induced by cue-based simulations. Nevertheless, EEG alone has successfully detected rest replay using a task similar to Liu, et al.6, where significant reverse replay during rest was linked to value learning, underscoring the capacity of EEG to detect rest replay signals²⁷. Another plausible explanation for the absence of rest-replay is the relatively simple sequence set-up, where subjects had less need to replay a sequence that is already well learnt. This contrast with the more demanding task features in Liu, et al.⁶ and Yu, et al.²⁷. This conjecture is supported by the near-perfect behavioral performance in the final run of sequence learning and is also consistent with Wimmer, et al.³¹, who reported enhanced mean reactivation, but not sequential replay, for well-encoded memories. However, it is also the case that stronger replay has been observed for sequences that have been more robustly encoded. For instance, the more time an animal spends within two place fields, the more frequently a corresponding place cell pair is reactivated during sleep⁶⁸. Conversely, other findings in the animal literature indicate that replay is more readily observed in novel compared to familiar tracks¹⁰, with a higher reactivation probability in novel environments⁶⁹. This raises an intriguing question regarding the relationship between learning performance and replay strength, particularly considering previous human studies report replay tends to prioritize weakly encoded memories⁵⁸. It is conceivable that the learning experience and replay strength follow an inverted U-shaped curve, where the strongest replay occurring for intermediate learning experience^{31,70}, a possibility that warrants more detailed investigation.

Comparing EEG and fMRI-based decoding, we found higher decoding accuracy for fMRI-based classifiers compared to EEG, possibly due to the much larger feature size. However, the reactivation/ replay analysis on the fMRI signal alone was less effective. During mental simulation, following Wittkuhn and Schuck²⁸, we found a qualitatively similar pattern to EEG-based replay, but this was nonsignificant in the fMRI signal (Fig. 4c). During rest, we found a chance level of decoding accuracy in hippocampus, and non-significant replay in hippocampus and mPFC, when applying the Schuck and Niv²⁴ method (Supplementary Fig. 6). This might reflect that mental imagery is a degraded, fuzzy experience, difficult to detect (Pearson, 2019), and these fMRI-based replay methods^{24,28,43} are not optimized for discerning replay events in the current study.

A question arising is whether EEG-based and fMRI-based analyses capture overlapping or independent cognitive processes. We found a significant positive correlation between decoding accuracy of EEG and fMRI classifiers during the functional localizer session, suggesting they capture a common process. However, at the level of reactivation dynamics, we found no temporal correlations between EEG and fMRI, neither during mental simulation nor during rest (Supplementary Fig. 10). When we probed the relationship between EEG and fMRI-

based reactivation in explaining hippocampal activation, we found a positive correlation during POST but not PRE Rest (Fig. 5g). This suggests that despite the different temporal dynamics between EEG and fMRI activity, spontaneous task-related reactivations align in the hippocampus. Furthermore, a stronger hippocampal BOLD activity when aligning to the onsets of EEG-based, as opposed to fMRI-based, reactivations (Fig. 5d), suggests that EEG may be more sensitive for localizing the timing of spontaneous task reactivations. Together, these findings imply that simultaneous EEG-fMRI can capture spontaneous cognitive processes, even when these are temporally transient or spatially distributed.

Lastly, research on reactivation and its sequential replay in humans is relatively nascent and has been significantly influenced by studies in rodents²⁵. While our human findings largely align with the rodent literature, it is also important to note the differences, as discussed above. The definition of replay or reactivation in humans predominantly refers to a representational frame of reference (e.g., 'brain representation of a face') as opposed to a neuronal level framework (e.g., place cells) in rodent studies. This distinction has implications for interpreting replay results, particularly regarding their brain-wide propagation. It is conceivable that representation results may not directly correspond to findings at the neuronal level, and vice versa. Future investigations, recording simultaneous neuronal activity in specific regions of the human brain, will be valuable in addressing this issue. For example, Staresina, et al.71 used intracranial electroencephalography combined with multiunit activity recordings from the human hippocampus and surrounding medial temporal lobe areas. They report a triple coupling between slow oscillations, spindles, and ripples, orchestrating neuronal processing for systemic consolidation during sleep, thereby validating results from rodent studies⁷².

In conclusion, using simultaneous EEG-fMRI, our study provides empirical validation of an analysis pipeline for studying replay and reactivation alongside whole-brain activation. Identifying the putative replay/reactivation events in EEG provides a unique timestamp for imaging brain-wide activation in fMRI. This same analysis pipeline helps bridge between disparate research areas and provides for a comprehensive understanding of the functions of replay in relation to human cognition. This opens exciting new possibilities for future studies, such as investigating hippocampal replay and grid-like coding during cognitive-map-based computation^{6,37}, as well as a richer examination of memory consolidation during sleep²⁵. It enables a more sophisticated understanding of the entorhinal-hippocampal-prefrontal systems underlying inference and generalization.

Methods

Participants

A total of 40 healthy adults were recruited for the study. All participants had normal or corrected-to-normal vision and no history of psychiatric or neurological disorders. They were screened for magnetic resonance imaging (MRI) eligibility prior to participation. The experiment was approved by the Medical Ethics Committee of Shenzhen University Medical School (reference number: PN-202300012), and all subjects provided written informed consent. After excluding subjects with excessive head motion (FD > 0.2) or incomplete participation, 33 subjects were included in the full analysis (age: 22.91 ± 0.33 years, 17 females, 16 males). None of the subjects reported any prior experience with the stimuli or the behavioral task.

Task

Overview of the task design. After completing preparatory work, subjects were taken into the MRI scanner. We began with a short brain localizer, followed by an 8-min anatomical scan and a 5-min resting-state scan, during which subjects were asked to stay awake and focus on a white fixation cross presented on a grey screen. Then, the subjects underwent a series of task sessions: functional localizer, sequence

learning, and cued mental simulation. We acquired four functional localizer runs of approximately 12 min each, three sequence learning runs of 6 min each. After sequence learning, we acquired a further 5-min resting-state, again with subjects' eye open. Finally, we acquired three cued mental simulation runs of about 10 min. The entire experiment lasted, on average, between 2 and 3 h.

Functional localizer. The functional localizer session was designed to train neural decoders on task states. The experiment utilized four visual stimuli (face, scissor, zebra, and banana), which were previously shown to elicit object-specific neural patterns in human brain^{3,45}. Subjects were presented with one of four images for 1sec and encouraged to consider its semantic content. Following this, a word was displayed for 1 sec, after a blank interval of 1-2 secs. Subjects then determined whether the word matched the preceding image, pressing '1' for matches and '2' for non-matches. Key positions were counterbalanced across subjects. Trials were separated with intervals of 1-3 secs to ensure adequate time delay between them. For incorrect responses, subjects received visual feedback for 1 sec. Each visual stimulus was shown 72 times, followed by both matching and nonmatching semantic stimuli, totaling 288 trials evenly split between corresponding and non-corresponding pairs. Stimuli were presented in a pseudo-random order, avoiding more than two consecutive presentations of the same stimulus. We provided visual feedback on the accuracy and timeliness of responses. Incorrect responses prompted feedback for 1 sec with instructions to press the correct button. If no response was made within the allotted time, a "Response timeout. Please answer promptly." message was displayed. For correct responses, no additional feedback was given, and the task moved to the next trial. Subjects achieving over 90% accuracy received a ¥20 bonus. The task comprised four blocks, each lasting about 12 min, totalling approximately 48 min for the entire task phase.

Sequence learning. In sequence learning session, subjects were required to build a 4-item sequence (e.g., $A \rightarrow B \rightarrow C \rightarrow D$) by mentally connecting three pairwise experiences (i.e., $A \rightarrow B$, $B \rightarrow C$, $C \rightarrow D$). The task comprised three runs, each including an associative learning (with three learning pairs) and a probe test. During learning, each trial started with a 300 ms fixation, then stimuli within the learning pair were presented sequentially, one for 1.5 s, with a 1-3 s interval between stimuli. The interval between learning pairs was 5 s. Each learning pair was repeated three times in a run. Subjects were asked to learn associations between stimuli, and their memory performances were probed in the following test. During test, a target stimulus with '->...->...?' cue was presented for 4s, and subjects were asked to imagine all images that followed the target image. Then after a 1-3 s interval with a blank screen, subjects were presented with a probe stimulus for 2 s. Subjects pressed key '1' if the probe stimulus followed the target stimulus in the sequence, and '2' otherwise. Key positions were counterbalanced between subjects, and no feedback was given during probe trials. There were 12 probe trials per learning run. The mapping between stimuli (face, scissor, zebra, and banana) and states (A, B, C, D) was fixed within subject but randomized across subjects. Subjects were allowed to proceed if they achieved at least 90% accuracy on the last learning run. Each block, consisting of one learning session and one test session, lasts about 6 min. With three blocks per subject, the total duration for this phase is approximately 18 min.

Cued mental simulation. Subjects were directed to mentally simulate the image sequence for $10 \, \text{s}$, in either a forward $(1 \rightarrow)$ or a reverse direction (\leftarrow 4) based upon a directional cue. Then, following a 1-3 s inter-stimulus interval, a probe image was displayed for 2 s. Subjects were required to determine whether the probe image was within the learnt sequence or not. To promote attentive processing, we created four *lure* probe images of the same content with the original ones, but

with subtle difference (e.g., orientation of the zebra head, colour of the banana, etc), as well as four new images with different content. The probe images were randomly displayed, with half necessitating a key '1' response if they were in the sequence, and the remaining half requiring a key '2' response if they were not. Key positions '1' and '2' were counterbalanced between subjects. No feedback was provided during probe trials to prevent additional learning. We found no difference of performance in differentiating original and lure images ($t_{(32)} = 0.62$, P = 0.541), suggesting the subjects were attentive. After probe test, participants were asked to assess the vividness of their recently performed mental simulation. The task comprised of 96 trials, equally split between forward and backward conditions. Each block, consisting of 32 trials, lasted about 10 min. With three blocks per subject, the total duration for an individual amounted to approximately 30 min.

EEG data acquisition

EEG was recorded simultaneously with fMRI data using an MR-compatible EEG amplifier system (BrainAmps MR-Plus, Brain Products, Germany), along with a specialized electrode cap (BrainCap). The recording was done using 64 channels using the international 10/20 system, with the reference channel positioned at FCz. A drop-down rear electrode was utilized to record electrocardiographic (ECG) activity. EEG data was recorded at a sample rate of 1000 Hz, with the impedance of all channels was kept below 10 k Ω throughout the experiment. To synchronize the EEG and fMRI recordings, the Brain-Vision recording software (BrainProducts, Germany) was utilized to capture triggers from both the MRI scanner and a stimulus presentation software developed using PsychoPy⁷³.

MRI data acquisition

All MRI data were acquired using a 64-channel head coil on a researchdedicated 3-Tesla Siemens Magnetom Prisma MRI scanner. For the functional scans, whole-brain images were acquired using a segmented k-space and steady-state T2*-weighted multi-band (MB) echo-planar imaging (EPI) single-echo gradient sequence that is sensitive to the BOLD contrast. This measures local magnetic changes caused by changes in blood oxygenation that accompany neural activity (sequence specification: 46 slices in interleaved ascending order: anterior-to-posterior (A-P) phase-encoding direction; TR = 1300 ms; echo time (TE) = 24 ms; voxel size = $3 \times 3 \times 3$ mm; matrix = 64×64 ; field of view (FOV) = 192×192 mm²; flip angle (FA) = 67° ; distance factor = 0%; MB acceleration factor 2). Slices were tilted for each subject by 30° forwards relative to the rostro-caudal axis to improve the quality of fMRI signal from the hippocampus. For each functional run, the task began after acquisition of the first four volumes (i.e., after 5.2 s) to avoid partial saturation effects and allow for scanner equilibrium. We also recorded two functional runs of resting-state fMRI data, one before and one after the functional localizer and sequence learning task runs. Each resting-state run was about 5 min in length, during which 237 functional volumes were acquired. High-resolution T1weighted (T1w) anatomical Magnetization Prepared Rapid Gradient Echo (MPRAGE) sequences were obtained from each subject to allow registration and brain-surface reconstruction (sequence specification: 192 slices; TR = 2300 ms; TE = 2.26 ms; $FA = 8^{\circ}$; inversion time (TI) = 1000 ms; matrix size = 192×256 ; FOV = 192×256 mm²; voxel size = 1×1000 $1 \times 1 \,\mathrm{mm}$).

EEG data preparation and preprocessing

EEG data collected inside MRI scanner was contaminated by imaging, ballistocardiographic and ocular artifacts. We utilized an Average Artefact Subtraction (AAS)⁷⁴ algorithm provide by the BrainVision Analyzer software (BrainProducts, Germany) to remove imaging artifacts. Following this, several preprocessing steps were undertaken, which involved removing residual physiological artifacts through the use of EEGLAB⁷⁵ and custom MATLAB scripts. We follow the same pre-

processing pipeline for previous MEG/EEG based replay analysis^{6,27,43}. Specifically, we downsampled the EEG data to a frequency of 100 Hz and applied 1 Hz high pass and 40 Hz low pass finite impulse response (FIR) filters. Due to poor signal quality, channel AF3 was excluded from further analysis, and the ECG channel was also excluded. To reduce dependence on the reference electrode position, the average of all electrodes was subtracted from each electrode. The data was then segmented into epochs extending from -200 ms before to 800 ms after the onset of functional localizer stimulus, and from -0.2 s before to 10 s after the onset of the mental simulation cue. To promote better decoding performance, baseline correction was omitted (see Supplementary Fig. 1b). Epochs showing residual MR artifacts were detected and removed from the dataset, with an average of 8.88 ± 0.39 (mean ± SEM) trials excluded for the functional localizer task and 9.12 ± 0.17 trials for the mental simulation task. Subsequently, Independent Component Analysis (ICA) was applied to the EEG data to isolate physiological artifacts from eye movements, muscle activity, and ballistocardiogram. These artifact-related ICs were carefully labeled and manually removed. EEG data during rest underwent the same preprocessing steps.

MRI data preparation and preprocessing

Results in this manuscript come from preprocessing performed using *fMRIPrep* 21.0.2 (Esteban, et al.⁷⁶; RRID:SCR_016216), which is based on *Nipype* 1.6.1 (Gorgolewski, et al.⁷⁷; RRID:SCR_002502). Many internal operations of *fMRIPrep* use *Nilearn* 0.8.1 (Abraham, et al.⁷⁸, RRID:SCR_001362), mostly within the functional processing workflow. For more details of the pipeline, see https://fmriprep.readthedocs.io/en/latest/workflows.html.

Conversion of data to the brain imaging data structure standard. To facilitate further analysis and sharing of data, all study data were arranged according to the Brain Imaging Data Structure (BIDS) specification using *dcm2bids* tool, which is freely available from https://unfmontreal.github.io/Dcm2Bids/.

Anatomical data preprocessing. One T1-weighted (T1w) image was found within the input BIDS dataset. The T1-weighted (T1w) was corrected for intensity non-uniformity (INU) N4BiasFieldCorrection⁷⁹, with with distributed **ANTs** 2.3.3 (RRID:SCR_004757)80, and used as T1w-reference throughout the workflow. The T1w-reference was then skull-stripped with a Nipype implementation of the antsBrainExtraction.sh workflow (from ANTs), using OASIS30ANTs as target template. Brain tissue segmentation of cerebrospinal fluid (CSF), white-matter (WM) and gray-matter (GM) was performed on the brain-extracted T1w using fast (FSL 6.0.5.1:57b01774, RRID:SCR_002823)81. Brain surfaces were reconstructed using recon-all (FreeSurfer 6.0.1, RRID:SCR_001847)82, and the brain mask estimated previously was refined with a custom variation of the method to reconcile ANTs-derived and FreeSurferderived segmentations of the cortical gray-matter of Mindboggle (RRID:SCR 002438)83. Volume-based spatial normalization to one standard space (MNI152NLin2009cAsym) was performed through nonlinear registration with antsRegistration (ANTs 2.3.3), using brainextracted versions of both T1w reference and the T1w template. The following template was selected for spatial normalization: ICBM 152 Nonlinear Asymmetrical template version 2009c [RRID:SCR 008796; TemplateFlow ID: MNI152NLin2009cAsym]84.

Functional data preprocessing. For each of the 12 BOLD runs found per subject (across all tasks and sessions), the following preprocessing was performed. First, a reference volume and its skull-stripped version were generated using a custom methodology of *fMRIPrep*. Headmotion parameters with respect to the BOLD reference (transformation matrices, and six corresponding rotation and translation

parameters) are estimated before any spatiotemporal filtering using mcflirt (FSL 6.0.5.1:57b01774)85. BOLD runs were slice-time corrected to 0.612 s (0.5 of slice acquisition range 0 s - 1.23 s) using 3dTshift from AFNI (RRID:SCR_005927)86. The BOLD time-series (including slicetiming correction when applied) were resampled onto their original, native space by applying the transforms to correct for head-motion. These resampled BOLD time-series will be referred to as preprocessed BOLD in original space, or just preprocessed BOLD. The BOLD reference was then co-registered to the T1w reference using bbregister (Free-Surfer) which implements boundary-based registration⁸⁷. Coregistration was configured with six degrees of freedom. Several confounding time-series were calculated based on the preprocessed BOLD: framewise displacement (FD), DVARS and three region-wise global signals. FD was computed using two formulations following Power (absolute sum of relative motions)⁸⁸ and Jenkinson (relative root mean square displacement between affines)85. FD and DVARS are calculated for each functional run, both using their implementations in Nipype (following the definitions by Power, et al.)88. The three global signals are extracted within the CSF, the WM, and the whole-brain masks. Additionally, a set of physiological regressors were extracted to allow for component-based noise correction (CompCor)89. Principal components are estimated after high-pass filtering the preprocessed BOLD time-series (using a discrete cosine filter with 128 s cut-off) for the two CompCor variants: temporal (tCompCor) and anatomical (aCompCor). tCompCor components are then calculated from the top 2% variable voxels within the brain mask. For aCompCor, three probabilistic masks (CSF, WM and combined CSF + WM) are generated in anatomical space. The implementation differs from that of Behzadi et al. in that instead of eroding the masks by 2 pixels on BOLD space, the aCompCor masks are subtracted a mask of pixels that likely contain a volume fraction of GM. This mask is obtained by dilating a GM mask extracted from the FreeSurfer's aseg segmentation, and it ensures components are not extracted from voxels containing a minimal fraction of GM. Finally, these masks are resampled into BOLD space and binarized by thresholding at 0.99 (as in the original implementation). Components are also calculated separately within the WM and CSF masks. For each CompCor decomposition, the k components with the largest singular values are retained, such that the retained components' time series are sufficient to explain 50 percent of variance across the nuisance mask (CSF, WM, combined, or temporal). The remaining components are dropped from consideration. The head-motion estimates calculated in the correction step were also placed within the corresponding confounds file. The confound time series derived from head motion estimates and global signals were expanded with the inclusion of temporal derivatives and quadratic terms for each 90. Frames that exceeded a threshold of 0.5 mm FD or 1.5 standardised DVARS were annotated as motion outliers.

The BOLD time-series were resampled into standard space, generating a *preprocessed BOLD run in MNII52NLin2O09cAsym space*. First, a reference volume and its skull-stripped version were generated using a custom methodology of *fMRIPrep*. The BOLD time-series were resampled onto the following surfaces (FreeSurfer reconstruction nomenclature): *fsnative, fsaverage*. All resamplings can be performed with *a single interpolation step* by composing all the pertinent transformations (i.e., head-motion transform matrices, susceptibility distortion correction when available, and co-registrations to anatomical and output spaces). Gridded (volumetric) resamplings were performed using antsApplyTransforms (ANTs), configured with Lanczos interpolation to minimize the smoothing effects of other kernels⁹¹. Non-gridded (surface) resamplings were performed using mri_vol2surf (FreeSurfer).

Multivariate EEG pattern analysis

Lasso-regularized logistic regression models were trained on EEG data elicited by direct presentations of the images. The preprocessed data

from 62 channels were used as input features for the model, which was implemented using the lassoglm function in MATLAB. Each model k had a vector of n+1 coefficients: one slope for each channel and one intercept. To prevent overfitting, we applied L1 regularization with a lambda coefficient of 0.001. To evaluate the performance of the model, 5-fold cross-validation was employed. The data were randomly divided into five equal-sized subsets, and the model was trained on four subsets and tested on the remaining subset. This process was repeated five times, with each subset serving as the test set once. Decoding accuracy was calculated as the number of correctly classified images divided by the total number of images. We performed decoding at one subject and one time point at a time, repeating the process several times to obtain decoding accuracy for all subjects throughout the entire epoch. We calculated the mean decoding accuracy across subjects to identify the peak decoding accuracy time point at the group level. This accuracy was then compared to a chance baseline of 25% using a two-sided one-sample t-test. We then selected the models corresponding to the time point with the highest accuracy to decode replay or mental simulation.

Multivariate fMRI pattern analysis

All fMRI pattern classification analyses were conducted using opensource packages from the Python (v.3.9.13) modules Nilearn (v.0.10.0)⁷⁸ and scikit-learn (version 1.1.2)⁹². All multiple comparison correction in fMRI analysis were performed using FMRIB Software Library (FSL, https://fsl.fmrib.ox.ac.uk/fsl/fslwiki/)⁹³.

Feature selection. Follow Wittkuhn and Schuck²⁸, we combined a functional ROI approach using thresholded t-maps and anatomical masks to identify image-responsive voxels located within a specific brain region. We ran four first-level general linear models (GLMs) for each subject, with one for each of the four cross-validation folds to identify voxels that showed significant activation in response to functional localizer by thresholding t-maps. A first-level GLM was fitted to the training set data (e.g., data from run 2 to 4) of each crossvalidation fold and modelled the visual stimulus onset of all corrected trials of functional localizer (1 s for all events). We included wrong trials as a regressor of no interest. All the parameters of GLM analysis were consistent with those utilized in other GLMs (see detail in GLM analysis part). These anatomical masks were created based on automated anatomical labelling for brain-surface reconstructions of individual T1w-reference images using Freesurfer^{82,94,95}, including the cuneus, lateral occipital sulcus, superior parietal lobule, pericalcarine gyrus, lingual gyrus, inferior parietal lobule, fusiform gyrus, inferior temporal gyrus, the middle temporal gyrus (cf. 31,96), as well as hippocampus, entorhinal cortex, and para hippocampal gyrus. Only gray-matter voxels were included in the masks⁹⁷. Voxels with t-values above or below a threshold of t = 3 in the anatomical mask for the left-out run (e.g., run 1) of the classification analysis were selected and set to 1 to create the final binarized masks.

Leave-one-run-out cross validation procedure. We performed fMRI pattern classification using a leave-one-run-out cross-validation approach, where three task runs (e.g., run 2 to 4) were used for training and the left-out runs (e.g., run 1) used for testing. We trained and tested the classifiers on data obtained from the trials where subjects responded correctly. Four independent one-vs-rest logistic regression classifiers were trained, one for each of the four stimulus classes (*face, scissor, zebra, banana*) and relabeled all other classes to a common *other* category. This process was repeated four times to ensure each task run served as the test set once. All the identical parameter settings were the consistent with those set by Wittkuhn and Schuck²⁸.

To identify the reactivation probability during mental simulation and rest period, we used all the data from functional localizer runs to train the classifiers. We created a new binarized mask for each subject by taking the intersection of the four binarized masks used for cross-validation. The classifiers with the same identical parameter settings as above were trained on the fMRI data. The classifiers were applied to the data during mental simulation (8 volumes per trial), and to data from resting sessions (230 volumes per rest session).

Temporally delayed linear modelling

We used Temporally Delayed Linear Modelling (TDLM) to measure spontaneous sequential reactivation of four states, either during the mental simulation or rest 43 . At each time bin during the mental simulation and the two resting sessions, we applied four classifiers to the EEG data and another four classifiers to the fMRI data. Each of these modality data sets contained three [time \times state] reactivation probability matrices from the mental simulation (three runs of mental simulation) and two reactivation probability matrices from the resting sessions (PRE and POST Rest).

In a first step, we aimed to identify evidence of state-to-state transitions at a given time $\log \Delta t$, by regressing a time-lagged copy of one state, X_j , onto another, X_k . In other words, the values of all states X_k at time t are used in a single multilinear model to predict the value of the single state X_j at time $t + \Delta t$:

$$X_{j}(t + \Delta t) = \sum_{k=1}^{n} X_{k}(t)\beta_{kj}$$
 (1)

In the second step, we tested for the strength of a particular hypothesized sequence, specified as a transition matrix, T:

$$\beta = \sum_{r=1}^{r} Z(r) \times T_r \tag{2}$$

 β is the [state × state] empirical transition matrix obtained from previous formula by ordinary least squares regression. T_r is hypothesized transition matrix. In our study, the transition matrices include a forward transition matrix, a backward transition matrix, a diagonal matrix and a constant matrix. Sequenceness, denoted as Z(r), reflected the strength of hypothesized transitions in the empirical matrices, which describe the degree to which representations were reactivated in a task-defined sequential order^{3,6,30,31,45}. Z_F and Z_R represented the forward and backward sequenceness, respectively. By repeating this regression at each time lag, we obtained time courses of sequenceness as a function of time lag. In our research, EEG had a time resolution of 10 ms, the smallest time lag in EEG-based TDLM (Fig. 4b, Supplementary Fig. 8), while fMRI had a time resolution of 1.3 s (1 TR), the smallest time lag in fMRI-based TDLM (Fig. 4a, Supplementary Fig. 5 & 8). Notably, because it is a linear modelling framework applied directly to concatenated, rather than individual replay onsets, TDLM does not distinguish effects of whole sequences from individual duplets. Essentially, it evaluates the average replay strength across all duplets during the whole period of interest.

We employed a non-parametric permutation-based method to test for statistical significance in this study. For each permutation, sequenceness was averaged across trials within each subject, and then across subjects. The null distribution was generated by randomly shuffling the rows and columns of the T_F (forward predictor matrix), with T_B (backward predictor matrix) being its transpose, and recalculating the second-level analysis for each shuffle. The permutations covered all possible combinations. For each permutation, the peak absolute mean sequence strength across participants and lags was calculated, controlling for multiple comparisons across lags. In the original, unpermuted data, sequence strength was deemed significant at a peak-level FWE < 0.05 if its value surpassed 95% of the peaks within the permutations. This method has been rigorously validated by simulation studies and empirical data in prior research^{3,6,31,43}. As previous human studies have only found evidence for replay with

relatively short lags^{3,6,30,43,45}, we visualized results up to a lag of 600 ms in EEG. To explore whether replay can be observed at longer time-scales, we extended the scale of time lag to 2000 ms. Simultaneously, we investigated the possibility of detecting replay in fMRI by computing the sequenceness using TDLM with a lag of up to 8 TR.

Identifying reactivation and replay onsets

To investigate the neural mechanisms underlying replay and task-related reactivation during the mental simulation and rest, we identified the onset of replay and task reactivation for subsequent parametric modulation and psychophysiological interaction analyses (Fig. 2b)^{30,45}. We used classifiers trained on functional localizer to decode the reactivation probability of each visual stimulus, resulting in a [time × state] reactivation matrix. Our analysis revealed a time lag of 30 ms between stimuli that provided the strongest evidence of replay transitions in the cued mental simulation task, as determined by TDLM (Fig. 4b). Next, we identified time points during mental simulation, where strong reactivation of one stimulus (e.g., A) was followed 30 ms later by strong reactivation of a structurally-adjacent stimulus (e.g., B). We first generated a matrix *Orig* as

$$Orig = X \times T \tag{3}$$

where X is the [time \times state] reactivation matrix, and T is the task transition matrix. The transition matrix T defines the mapping between the task state corresponding to column i in X, and column i in Orig (specifically, column i in Orig is the reactivation time course of the state that 'precedes' state i in T). We then shifted each column of X by $\Delta_t = 30$ ms, to generate another matrix Proj,

$$Proj = X(\Delta t)$$
 (4)

where row i of Proj correspond to row i+30 ms of X. Multiplying Proj and Orig elementwise, and summing over the columns of the resulting matrix, giving a total of k states, to obtain a long [time \times 1] vector, R. Each element in the R indicates the strength of two-state replay at a given moment in time.

$$R_t = \sum_{i=1}^k Orig_{ti} \times Proj_{ti}$$
 (5)

Based on this approach, we calculated forward and backward replay probability onsets for each time point during mental simulation. The replay probability in our study was formed by 30-ms-time-lag forward replay in both forward and backward mental simulation conditions. We convolved the replay probability onsets with the HRF, and downsampled it to the same temporal resolution with fMRI signal. The resulting replay probability onset was an EEG-based replay probability onset regressor.

The same analysis pipeline was applied to EEG-based task reactivation probability during both PRE Rest and POST Rest periods. To compare reactivation strength between PRE and POST Rest, we averaged reactivation probabilities across all time points and task stimuli for each rest period, defining this as the mean reactivation strength for each period. Recognizing that spontaneous thoughts could lead to spurious reactivation in both PRE and POST Rest periods. Thus, as a chance level cannot be established a priori, we opt to use the reactivation level during the PRE Rest period as a benchmark for assessing reactivation during the POST Rest.

Detecting neural sequence in task-based fMRI patterns

We employed Wittkuhn and Schuck's method²⁸ to measure neural sequence in fMRI data during mental simulation. In brief, this involves identifying the relationship between image position in the sequence and task reactivation probability based on an fMRI decoding classifier.

Task reactivation probability during cued mental simulation was normalized by dividing them by their trial-wise sum for each stimulus. Subsequently, we conducted a linear regression between the serial position of four images and their normalized decoding probabilities at every TR. The slopes of linear regression were averaged at the subject level for each task condition and each TR. The sign of the mean regression slopes was flipped so that positive values indicate forward ordering and negative values indicate backward ordering. We also performed the two-sided one-sample t-tests to compare the mean regression slope coefficients against zero for each TR and adjusted their *P* values by multiple comparison correction (Fig. 4a for illustration, Fig. 4c for observed data).

It is worth noting that in our study, the [time × state] reactivation probability matrices came from the sequential mental simulation, not sequential visual presentation. Since we could not identify the time at which subjects imagined each image or the speed of imagination, we cannot predict probability differences between two time-shifted events by sinusoidal response functions from Wittkuhn and Schuck²⁸. The junction of the 1st and 2nd period was defined as the point at which the regression slope crossed y = 0 in the forward mental simulation in the positive to negative direction (e.g., junction = 5.2 TR), with the 1^{st} period preceding the junction (e.g., 1^{st} period = [1, 2, 3, 4, 5] TR) and the 2^{nd} period following it (e.g., 2^{nd} period = [6, 7, 8] TR). Slope coefficients were averaged for each task condition and period (Fig. 4a for illustration, the bar plots in the upper right corner of the Fig. 4c for emperical data). We conducted the two-sided one-sample t-tests to compare the mean regression slopes against zero for each task condition and period.

Detecting sequential replay in rest-based fMRI patterns

We employed Schuck and Niv's method²⁴ to measure sequential replay in fMRI data acquired during rest. This method involves identifying the relationship between transition frequency between states and state distances. Similar to the aforementioned training of decoding classifiers (refer to Multivariate fMRI pattern analysis section), hippocampus and mPFC anatomical masks were created based on automated anatomical labelling for brain-surface reconstructions of individual T1wreference images using Freesurfer^{82,94,95}. We selected the corresponding labels of the bilateral medial orbitofrontal, rostral anterior cingulate, and superior frontal regions for the anatomical mask of mPFC, and the corresponding labels of the bilateral hippocampus regions for the anatomical mask of hippocampus. Considering that these two masks consist of small-quantity voxels, we didn't employed the thresholded t-map to select image-responsive voxels²⁸. Based on the decoding accuracy, the classifiers trained in mPFC mask at the 5th TR after stimulus onset were chosen to predict the probabilities during mental simulation and rest (see Supplementary Fig. 8).

For each task condition (forward and backward mental simulation) and each rest session (PRE and POST Rest), we selected 230 TRs time series of decoding probabilities. This resulted in 229 state transitions for each condition, allowing us to calculate the transition frequency. Similar to Schuck and Niv²⁴, We conducted a logistic mixed-effects analysis to examine the effects of state distances (hypothesized transition matrix) on transition frequency between states (empirical transition matrix) while simultaneously excluding the different sources of between- and within-participant variability. To compare the models, we employed a likelihood ratio test, comparing a logistic regression model that solely included random effects to a model that also incorporated the state distances regressor.

GLM analysis

We performed the GLMs to capture the significant event related activations in various sessions: functional localizer (GLM 1), sequence learning (GLM 2, GLM 3), cued mental simulation (GLM 4) and rest periods (GLM 5 for EEG-based reactivation, GLM 6 for fMRI-based

reactivation). The fMRI data were smoothed with a 6 mm FWHM kernel before group-level statistics were performed in the GLMs. All images underwent high pass filtering in the temporal domain (width 128 s), and autocorrelation of the hemodynamic responses was modelled using an AR (1) model. We included nuisance regressors estimated during preprocessing with fMRIprep: the six rigid-body motion-correction parameters estimated during realignment (three translation and rotation parameters, respectively), mean White Matter, and mean Cerebral Spinal Fluid. The effect of the experimental conditions on regional blood oxygenation level-dependent responses was estimated with the GLMs. For the group-level analysis, a one-sample t-test was conducted using the whole brain as the volume of interest, and paired t-test was conducted to compare the difference of whole brain activation between PRE Rest and POST Rest. All whole-brain analyses, with the exception for those mentioned otherwise, were thresholded and displayed using a cluster-wise family-wise error (FWE) correction P < 0.05, with cluster-forming threshold $P_{unc.} < 0.001$ at the voxel level, as reported by FSL.

GLM 1: the activation of images and semantic text in the functional localizer. GLM 1 was employed to find the activation of images and semantic text in the functional localizer session. Each run was modelled with ten regressors, including four regressors to model the onsets of four images, four regressors to model the onsets of four semantic text in correct response trials, one regressor to model the onsets of semantic texts in wrong response trials, and another regressor modelling the onsets of response. To obtain the mean activation of visual processing and semantic processing, we averaged the effect of four images and four semantic texts, respectively (Supplementary Fig. 2a, right panel for images, and Supplementary Fig. 2b, left panel for semantic texts). Furthermore, we identified the specific activation of stimuli by contrasting a specific image or semantic text with the other three images and texts (Supplementary Fig. 2a, left panel for images, and Supplementary Fig. 2b, right panel for semantic texts).

GLM 2: the contrast of 1st and 2nd image during sequence learning. GLM 2 was used to examine the differences of activation between the first and second images during sequence learning session. Each run was modelled with two regressors: (1) the onsets of the first image, (2) the onsets of the second image. We contrasted the effect of the first image with that of the second image in the first level GLM (Supplementary Fig. 3a).

GLM 3: the activation of target image and probe image in sequence probe test. GLM 3 was designed to investigate the activation of target image and probe image in the sequence probe test. Each run was modelled with four regressors: (1) the onsets of target image (Supplementary Fig. 3c), (2) the onsets of the response, (3) the onsets of correct probe image in all correct response trials, (4) the onsets of wrong probe image in all correct response trials. To access the effect of the wrong probe image in the probe test, we contrasted the effect of probe images between the wrong probe image and correct probe image in the first level GLM (Supplementary Fig. 3d).

Reactivation and replay onsets modulation analysis

GLM 4: the neural correlates of EEG-based replay during mental simulation. To investigate the neural correlates of replay events during mental simulation, we performed a GLM 4 with three regressors. The first regressor represented the onsets of EEG-based replay probability events (See *Identifying reactivation and replay onsets*). We added two more regressors to isolate the unique brain activations associated with replay. The second regressor modelled the duration of mental simulation in all correct-response trials, while the third regressor modelled the duration of mental simulation in all wrong-

response trials. These two regressors were modelled as boxcar functions with a duration of 10 s for all trials. We orthogonalized the first two regressors in GLM 4 to remove any shared variances so that the regression coefficients reflected the unique contribution of each regressor in explaining the variances in neural signals.

GLM 5: the neural correlates of EEG-based task reactivation in the resting states. To investigate the neural correlates of EEG-based task reactivation during rest, we conducted a GLM 5. We summed the [time * state] task-related reactivation probabilities across four task stimuli for each time point, resulting in a [time \times 1] array of EEG-based reactivation probability onsets. We convolved the [time \times 1] reactivation probability onsets with the HRF, and downsampled it to the same temporal resolution with fMRI signal. We added it as a psychological regressor to the design matrix of the GLM 5.

GLM 6: the neural correlates of fMRI-based task reactivation in the resting states. To investigate the neural correlates of fMRI-based task reactivation during rest, we performed a GLM 6. We summed the [time * state] task-related reactivation probabilities across four task stimuli for each time point, resulting in a [time × 1] array of fMRI-based reactivation probability onsets. As the fMRI-based reactivation itself has HRF properties, we added it as a psychological regressor to the design matrix of the GLM 6 without HRF convolution.

ROI analysis

The purpose of ROI analysis in our study is to identify the increased activation during PRE and POST Rest. The beta values at the subjectlevel for further statistical inference were averaged across all voxels within each ROI. The hippocampus ROI in our study was anatomically defined using a high-resolution probabilistic atlas of Harvard-Oxford Atlas⁹⁸. The primary motor cortex ROI in our study was anatomically defined using a high-resolution probabilistic atlas of Juelich Histological Atlas⁹⁹. In the further ROI analysis, any voxels that have any probability of being in the hippocampus and primary motor cortex were included in the ROIs. Two-sided one sample t-tests were performed on beta values for each ROI, rest ression and modality, while two-sided paired t-tests were conducted between rest sessions (PRE versus POST Rest) and modalities (EEG versus fMRI). Additionally, we defined entorhinal cortex ROI by applying 40% threshold to the Juelich Histological Atlas for PPI analysis between hippocampal activity and task reactivation during rest.

PPI analysis

We performed whole-brain PPI analyses using *nilearn* during mental simulation and rest periods. The first analysis aimed to study replay-triggered brain-wide activation during mental simulation. To achieve this, we used the same hippocampus ROI as the *ROI analysis*. The first PPI model included three regressors for replay onsets: (1) BOLD timeseries extracted from hippocampus, (2) the EEG-based replay probability, (3) the product of the above two regressors (Fig. 4e).

The second whole-brain PPI analysis aimed to study EEG- and fMRI-based task reactivation aligned brain-wide activation during rest periods. This PPI model included three regressors for task reactivation onsets: (1) BOLD timeseries extracted from hippocampus, (2) the EEG- or fMRI-based task reactivation probability, and (3) the product of the above two regressors (Fig. 5e).

Cross-correlation

Cross-correlation measures the similarity between two signals as a function of the time lag applied to one of the signals. In the context of EEG-based and fMRI-based decoding probability, during task and rest, we employed the cross-correlation by sliding the EEG time series across the fMRI time series at different time lags and computing the correlation coefficient at each lag. To ensure

compatibility between the two signals, we downsampled the EEG time series to the same temporal resolution with fMRI time series before calculating the cross-correlation. We used the cross-correlation function from Liu, et al.⁴³ and the time lag ranging from 1 to 8 TR in our analysis. The peak of the cross-correlation coefficient indicated the point at which the two signals demonstrated the highest degree of similarity. We also performed the two-sided one-sample t-tests to compare the cross-correlation coefficients against zero for each TR and adjusted their *P* values by multiple comparison correction (Supplementary Fig. 10).

Statistical analysis

Sample sizes were not determined using statistical methods, but were compared with those reported in previous research on replay^{3,6,28,32}. Statistical comparisons were performed using with appropriate inferential methods, as indicated in the figure captions. In cases where multiple hypothesis testing was applicable, we applied the correction method to correct for it^{100,101}.

Reporting summary

Further information on research design is available in the Nature Portfolio Reporting Summary linked to this article.

Data availability

The behavioural data, first-level and second-level fMRI statistical images, and EEG decoded time series generated in this study have been deposited in the Zenodo database. They can be found at https://zenodo.org/records/12547774. Source data are provided with this paper.

Code availability

The analysis code can be found at https://gitlab.com/liu_lab/EEG-fMRI-replay.git.

References

- Wilson, M. A. & McNaughton, B. L. Reactivation of hippocampal ensemble memories during sleep. Science 265, 676–679 (1994).
- Nádasdy, Z., Hirase, H., Czurkó, A., Csicsvari, J. & Buzsáki, G. Replay and time compression of recurring spike sequences in the hippocampus. J. Neurosci. 19, 9497–9507 (1999).
- 3. Liu, Y., Mattar, M. G., Behrens, T. E. J., Daw, N. D. & Dolan, R. J. Experience replay is associated with efficient nonlocal learning. *Science* **372**, eabf1357 (2021).
- Widloski, J. & Foster, D. J. Flexible rerouting of hippocampal replay sequences around changing barriers in the absence of global place field remapping. *Neuron* 110, 1547–1558 (2022).
- Schwartenbeck, P. et al. Generative replay for compositional visual understanding in the prefrontal-hippocampal circuit. Cell 186, 4885–4897.e4814 (2023).
- Liu, Y., Dolan, R. J., Kurth-Nelson, Z. & Behrens, T. E. J. Human replay spontaneously reorganizes experience. *Cell* 178, 640–652.e614 (2019).
- Gupta, A. S., van der Meer, M. A. A., Touretzky, D. S. & Redish, A. D. Hippocampal replay Is not a simple function of experience. *Neuron* 65, 695–705 (2010).
- 8. Schwartenbeck, P. et al. Computational mechanisms of curiosity and goal-directed exploration. *Elife* **8**, e41703 (2019).
- Sutherland, G. R. & McNaughton, B. Memory trace reactivation in hippocampal and neocortical neuronal ensembles. *Curr. Opin.* Neurobiol. 10, 180–186 (2000).
- Foster, D. J. & Wilson, M. A. Reverse replay of behavioural sequences in hippocampal place cells during the awake state. Nature 440, 680–683 (2006).
- Davidson, T. J., Kloosterman, F. & Wilson, M. A. Hippocampal replay of extended experience. Neuron 63, 497–507 (2009).

- Diba, K. & Buzsáki, G. Forward and reverse hippocampal place-cell sequences during ripples. Nat. Neurosci. 10, 1241-1242 (2007).
- Foster, D. J. Replay comes of age. Annu. Rev. Neurosci. 40, 581–602 (2017).
- Carr, M. F., Jadhav, S. P. & Frank, L. M. Hippocampal replay in the awake state: a potential substrate for memory consolidation and retrieval. *Nat. Neurosci.* 14, 147–153 (2011).
- Buzsáki, G. Hippocampal sharp wave-ripple: A cognitive biomarker for episodic memory and planning. *Hippocampus* 25, 1073–1188 (2015).
- Ambrose, R. E., Pfeiffer, B. E. & Foster, D. J. Reverse replay of hippocampal place cells is uniquely modulated by changing reward. *Neuron* 91, 1124–1136 (2016).
- Hahamy, A., Dubossarsky, H. & Behrens, T. E. J. The human brain reactivates context-specific past information at event boundaries of naturalistic experiences. *Nat. Neurosci.* 26, 1080–1089 (2023).
- Kaefer, K., Nardin, M., Blahna, K. & Csicsvari, J. Replay of behavioral sequences in the medial prefrontal cortex during rule switching. *Neuron* 106, 154–165 (2020).
- Ji, D. & Wilson, M. A. Coordinated memory replay in the visual cortex and hippocampus during sleep. *Nat. Neurosci.* 10, 100–107 (2007).
- O'Neill, J., Boccara, C. N., Stella, F., Schönenberger, P. & Csicsvari, J. Superficial layers of the medial entorhinal cortex replay independently of the hippocampus. Science 355, 184–188 (2017).
- Shanahan, L. K., Gjorgieva, E., Paller, K. A., Kahnt, T. & Gottfried, J. A. Odor-evoked category reactivation in human ventromedial prefrontal cortex during sleep promotes memory consolidation. elife 7, e39681 (2018).
- Tambini, A. & Davachi, L. Awake reactivation of prior experiences consolidates memories and biases cognition. *Trends Cogn. Sci.* 23, 876–890 (2019).
- Wang, B. et al. Targeted memory reactivation during sleep elicits neural signals related to learning content. *J. Neurosci.* 39, 6728–6736 (2019).
- 24. Schuck, N. W. & Niv, Y. Sequential replay of nonspatial task states in the human hippocampus. *Science* **364**, eaaw5181 (2019).
- Liu, Y., Nour, M. M., Schuck, N. W., Behrens, T. E. J. & Dolan, R. J. Decoding cognition from spontaneous neural activity. *Nat. Rev. Neurosci.* 23, 204–214 (2022).
- Kurth-Nelson, Z., Economides, M., Dolan, R. J. & Dayan, P. Fast sequences of non-spatial state representations in humans. *Neuron* 91, 194–204 (2016).
- 27. Yu, Q. et al. Reduced reverse replay in anxious individuals impairs reward prediction. *bioRxiv* (2023).
- Wittkuhn, L. & Schuck, N. W. Dynamics of fMRI patterns reflect sub-second activation sequences and reveal replay in human visual cortex. Nat. Commun. 12, 1795 (2021).
- Wittkuhn, L., Krippner, L. M. & Schuck, N. W. Statistical learning of successor representations is related to on-task replay. bioRxiv (2022).
- 30. Wimmer, G. E., Liu, Y., McNamee, D. C. & Dolan, R. J. Distinct replay signatures for prospective decision-making and memory preservation. *Proc. Natl Acad. Sci.* **120**, e2205211120 (2023).
- 31. Wimmer, G. E., Liu, Y., Vehar, N., Behrens, T. E. J. & Dolan, R. J. Episodic memory retrieval success is associated with rapid replay of episode content. *Nat. Neurosci.* **23**, 1025–1033 (2020).
- Higgins, C. et al. Replay bursts in humans coincide with activation of the default mode and parietal alpha networks. *Neuron* 109, 882–893.e887 (2021).
- 33. Whittington, J. C. R., McCaffary, D., Bakermans, J. J. W. & Behrens, T. E. J. How to build a cognitive map: insights from models of the hippocampal formation. *arXiv* (2022).
- Behrens, T. E. J. et al. What is a cognitive map? Organizing knowledge for flexible behavior. *Neuron* 100, 490-509 (2018).

- Raichle, M. E. & Snyder, A. Z. A default mode of brain function: A brief history of an evolving idea. *NeuroImage* 37, 1083–1090 (2007).
- Hassabis, D., Kumaran, D., Vann, S. D. & Maguire, E. A. Patients with hippocampal amnesia cannot imagine new experiences. *Proc. Natl Acad. Sci.* 104, 1726–1731 (2007).
- Constantinescu, A. O., O'Reilly, J. X. & Behrens, T. E. J. Organizing conceptual knowledge in humans with a gridlike code. Science 352, 1464–1468 (2016).
- Park, S. A., Miller, D. S. & Boorman, E. D. Inferences on a multidimensional social hierarchy use a grid-like code. *Nat. Neurosci.* 24, 1292–1301 (2021).
- Baldassano, C., Hasson, U. & Norman, K. A. Representation of realworld event schemas during narrative perception. J. Neurosci. 38, 9689–9699 (2018).
- Philiastides, M. G., Tu, T. & Sajda, P. Inferring macroscale brain dynamics via fusion of simultaneous EEG-fMRI. *Annu. Rev. Neu*rosci. 44, 315–334 (2021).
- Pisauro, M. A., Fouragnan, E., Retzler, C. & Philiastides, M. G. Neural correlates of evidence accumulation during value-based decisions revealed via simultaneous EEG-fMRI. *Nat. Commun.* 8, 15808 (2017).
- 42. Hauser, T. U. et al. The feedback-related negativity (FRN) revisited: New insights into the localization, meaning and network organization. *NeuroImage* **84**, 159–168 (2014).
- Liu, Y. et al. Temporally delayed linear modelling (TDLM) measures replay in both animals and humans. Elife 10, e66917 (2021).
- Friston, K. J. et al. Psychophysiological and modulatory interactions in neuroimaging. *NeuroImage* 6, 218–229 (1997).
- 45. Nour, M. M., Liu, Y., Arumuham, A., Kurth-Nelson, Z. & Dolan, R. J. Impaired neural replay of inferred relationships in schizophrenia. *Cell* **184**, 4315–4328.e4317 (2021).
- McFadyen, J., Liu, Y. & Dolan, R. J. Differential replay of reward and punishment paths predicts approach and avoidance. *Nat. Neu*rosci. 26, 627–637 (2023).
- Garvert, M. M., Dolan, R. J. & Behrens, T. E. J. A map of abstract relational knowledge in the human hippocampal-entorhinal cortex. eLife 6, e17086 (2017).
- 48. Karlsson, M. P. & Frank, L. M. Awake replay of remote experiences in the hippocampus. *Nat. Neurosci.* **12**, 913–918 (2009).
- Ólafsdóttir, H. F., Bush, D. & Barry, C. The role of hippocampal replay in memory and planning. Curr. Biol. 28, R37–R50 (2018).
- Klein-Flügge, M. C., Bongioanni, A. & Rushworth, M. F. S. Medial and orbital frontal cortex in decision-making and flexible behavior. Neuron 110, 2743–2770 (2022).
- Schapiro, A. C., Turk-Browne, N. B., Norman, K. A. & Botvinick, M. M. Statistical learning of temporal community structure in the hippocampus. *Hippocampus* 26, 3–8 (2016).
- Sherrill, K. R. et al. Generalization of cognitive maps across space and time. Cereb. Cortex 33, 7971–7992 (2023).
- Silston, B. et al. Neural encoding of perceived patch value during competitive and hazardous virtual foraging. *Nat. Commun.* 12, 5478 (2021).
- Baram, A. B., Muller, T. H., Nili, H., Garvert, M. M. & Behrens, T. E. J. Entorhinal and ventromedial prefrontal cortices abstract and generalize the structure of reinforcement learning problems. Neuron 109, 713–723.e717 (2021).
- 55. Vaidehi, S. N. et al. Stimulation of the posterior cingulate cortex impairs episodic memory encoding. *J. Neurosci.* **39**, 7173 (2019).
- Bone, M. B. & Buchsbaum, B. R. Detailed episodic memory depends on concurrent reactivation of basic visual features within the posterior hippocampus and early visual cortex. *Cereb. Cortex Commun.* 2, tgab045 (2021).
- Favila, S. E., Lee, H. & Kuhl, B. A. Transforming the concept of memory reactivation. *Trends Neurosci.* 43, 939–950 (2020).

- Schapiro, A. C., McDevitt, E. A., Rogers, T. T., Mednick, S. C. & Norman, K. A. Human hippocampal replay during rest prioritizes weakly learned information and predicts memory performance. *Nat. Commun.* 9, 3920 (2018).
- Agrawal, M., Mattar, M. G., Cohen, J. D. & Daw, N. D. The temporal dynamics of opportunity costs: A normative account of cognitive fatigue and boredom. *Psychol. Rev.* 129, 564 (2022).
- Kaplan, R. et al. Hippocampal sharp-wave ripples influence selective activation of the default mode network. *Curr. Biol.* 26, 686–691 (2016).
- 61. Liu, X. et al. Multimodal neural recordings with Neuro-FITM uncover diverse patterns of cortical-hippocampal interactions. *Nat. Neurosci.* **24**, 886–896 (2021).
- Nitzan, N., Swanson, R., Schmitz, D. & Buzsáki, G. Brain-wide interactions during hippocampal sharp wave ripples. *Proc. Natl Acad. Sci.* 119, e2200931119 (2022).
- Mattar, M. G. & Daw, N. D. Prioritized memory access explains planning and hippocampal replay. *Nat. Neurosci.* 21, 1609–1617 (2018).
- 64. Dijkstra, N. & Fleming, S. M. Subjective signal strength distinguishes reality from imagination. *Nat. Commun.* **14**, 1627 (2023).
- Aronov, D., Nevers, R. & Tank, D. W. Mapping of a non-spatial dimension by the hippocampal-entorhinal circuit. *Nature* 543, 719–722 (2017).
- Hafting, T., Fyhn, M., Molden, S., Moser, M.-B. & Moser, E. I.
 Microstructure of a spatial map in the entorhinal cortex. *Nature* 436, 801–806 (2005).
- Ólafsdóttir, H. F., Carpenter, F. & Barry, C. Coordinated grid and place cell replay during rest. Nat. Neurosci. 19, 792–794 (2016).
- O'Neill, J., Senior, T. J., Allen, K., Huxter, J. R. & Csicsvari, J. Reactivation of experience-dependent cell assembly patterns in the hippocampus. *Nat. Neurosci.* 11, 209–215 (2008).
- Cheng, S. & Frank, L. M. New experiences enhance coordinated neural activity in the hippocampus. *Neuron* 57, 303–313 (2008).
- Ritvo, V. J. H., Turk-Browne, N. B. & Norman, K. A. Nonmonotonic plasticity: how memory retrieval drives learning. *Trends Cogn. Sci.* 23, 726–742 (2019).
- Staresina, B. P., Niediek, J., Borger, V., Surges, R. & Mormann, F. How coupled slow oscillations, spindles and ripples coordinate neuronal processing and communication during human sleep. *Nat. Neurosci.* 26, 1429–1437 (2023).
- Klinzing, J. G., Niethard, N. & Born, J. Mechanisms of systems memory consolidation during sleep. *Nat. Neurosci.* 22, 1598–1610 (2019).
- 73. Peirce, J. et al. PsychoPy2: Experiments in behavior made easy. Behav. Res. methods **51**, 195–203 (2019).
- Allen, P. J., Josephs, O. & Turner, R. A method for removing imaging artifact from continuous EEG recorded during functional MRI. Neuroimage 12, 230–239 (2000).
- Delorme, A. & Makeig, S. EEGLAB: an open source toolbox for analysis of single-trial EEG dynamics including independent component analysis. J. Neurosci. Methods 134, 9–21 (2004).
- Esteban, O. et al. fMRIPrep: a robust preprocessing pipeline for functional MRI. Nat. Methods 16, 111–116 (2019).
- 77. Gorgolewski, K. et al. Nipype: a flexible, lightweight and extensible neuroimaging data processing framework in python. *Front. Neuroinform.* **5**, 13 (2011).
- Abraham, A. et al. Machine learning for neuroimaging with scikitlearn. Front. Neuroinform. 8, 14 (2014).
- 79. Tustison, N. J. et al. N4ITK: improved N3 bias correction. *IEEE Trans. Med. Imaging* **29**, 1310–1320 (2010).
- Avants, B. B., Epstein, C. L., Grossman, M. & Gee, J. C. Symmetric diffeomorphic image registration with cross-correlation: evaluating automated labeling of elderly and neurodegenerative brain. *Med. Image Anal.* 12, 26–41 (2008).

- 81. Zhang, Y., Brady, M. & Smith, S. Segmentation of brain MR images through a hidden Markov random field model and the expectation-maximization algorithm. *IEEE Trans. Med. Imaging* **20**, 45–57 (2001).
- Dale, A. M., Fischl, B. & Sereno, M. I. Cortical surface-based analysis: I. Segmentation and surface reconstruction. *Neuroimage* 9, 179–194 (1999).
- 83. Klein, A. et al. Mindboggling morphometry of human brains. *PLoS Computational Biol.* **13**, e1005350 (2017).
- Fonov, V. S., Evans, A. C., McKinstry, R. C., Almli, C. R. & Collins, D.
 L. Unbiased nonlinear average age-appropriate brain templates from birth to adulthood. *NeuroImage* 47, S102 (2009).
- 85. Jenkinson, M., Bannister, P., Brady, M. & Smith, S. Improved optimization for the robust and accurate linear registration and motion correction of brain images. *Neuroimage* 17, 825–841 (2002).
- Cox, R. W. & Hyde, J. S. Software tools for analysis and visualization of fMRI data. NMR Biomedicine: Int. J. Devot. Dev. App.Magn. Reson. Vivo 10, 171–178 (1997).
- 87. Greve, D. N. & Fischl, B. Accurate and robust brain image alignment using boundary-based registration. *Neuroimage* **48**, 63–72 (2009).
- Power, J. D. et al. Methods to detect, characterize, and remove motion artifact in resting state fMRI. *Neuroimage* 84, 320–341 (2014).
- Behzadi, Y., Restom, K., Liau, J. & Liu, T. T. A component based noise correction method (CompCor) for BOLD and perfusion based fMRI. Neuroimage 37, 90–101 (2007).
- Satterthwaite, T. D. et al. An improved framework for confound regression and filtering for control of motion artifact in the preprocessing of resting-state functional connectivity data. *Neuro*image 64, 240–256 (2013).
- 91. Lanczos, C. Evaluation of noisy data. J. Soc. Ind. Appl. Math., Ser. B: Numer. Anal. 1, 76–85 (1964).
- 92. Pedregosa, F. et al. Scikit-learn: Machine learning in Python. J. Mach. Learn. Res. 12. 2825–2830 (2011).
- 93. Smith, S. M. et al. Advances in functional and structural MR image analysis and implementation as FSL. *Neuroimage* **23**, S208–S219 (2004).
- Poldrack, R. A. Region of interest analysis for fMRI. Soc. Cogn. Affect. Neurosci. 2, 67–70 (2007).
- Fischl, B. et al. Automatically parcellating the human cerebral cortex. Cereb. Cortex 14, 11–22 (2004).
- Haxby, J. V. et al. Distributed and overlapping representations of faces and objects in ventral temporal cortex. Science 293, 2425–2430 (2001).
- Kunz, L., Deuker, L., Zhang, H. & Axmacher, N. in Handbook of Behavioral Neuroscience Vol. 28 Handbook of in Vivo Neural Plasticity Techniques In (ed Denise Manahan-Vaughan) 481–508 (Elsevier, 2018).
- 98. Desikan, R. S. et al. An automated labeling system for subdividing the human cerebral cortex on MRI scans into gyral based regions of interest. *NeuroImage* **31**, 968–980 (2006).
- 99. Eickhoff, S. B. et al. A new SPM toolbox for combining probabilistic cytoarchitectonic maps and functional imaging data. *NeuroImage* **25**, 1325–1335 (2005).
- 100. Benjamini, Y. Discovering the false discovery rate. *J. Royal Stat. Soc.: Series B (Stat. Methodology.)* **72**, 405–416 (2010).
- Lifanov, J. et al. Reconstructing spatio-temporal trajectories of visual object memories in the human brain. bioRxiv (2022).

Acknowledgements

This study is supported by the National Science and Technology Innovation 2030 Major Program (2022ZD0205500), the National Natural Science Foundation of China (32271093), the Beijing Natural Science Foundation (Z230010), the Major Project of the National Social Science

Foundation (20&ZD153), the Fundamental Research Funds for the Central Universities, and the Shenzhen-Hong Kong Institute of Brain Science – Shenzhen Fundamental Research Institutions (2022SHIBS0003). The authors also thank the Magnetic Resonance Imaging Center at Shenzhen University for providing the MRI scanning.

Author contributions

Conceptualization, Y.L., Q.H., Z.X., Q.Y., R.D., and T.B.; Investigation, Q.H., Z.X., Q.Y., Y.L., J.X., Y.Q., and Y.Luo.; Writing – Original Draft, Y.L., Q.H., Z.X.; Writing – Review & Editing, Y.L., Q.H., Z.X., R.D., and T.B.

Competing interests

The authors declare no competing interests.

Additional information

Supplementary information The online version contains supplementary material available at https://doi.org/10.1038/s41467-024-51582-5.

Correspondence and requests for materials should be addressed to Yunzhe Liu.

Peer review information *Nature Communications* thanks the anonymous reviewers for their contribution to the peer review of this work. A peer review file is available.

Reprints and permissions information is available at http://www.nature.com/reprints

Publisher's note Springer Nature remains neutral with regard to jurisdictional claims in published maps and institutional affiliations.

Open Access This article is licensed under a Creative Commons Attribution-NonCommercial-NoDerivatives 4.0 International License, which permits any non-commercial use, sharing, distribution and reproduction in any medium or format, as long as you give appropriate credit to the original author(s) and the source, provide a link to the Creative Commons licence, and indicate if you modified the licensed material. You do not have permission under this licence to share adapted material derived from this article or parts of it. The images or other third party material in this article are included in the article's Creative Commons licence, unless indicated otherwise in a credit line to the material. If material is not included in the article's Creative Commons licence and your intended use is not permitted by statutory regulation or exceeds the permitted use, you will need to obtain permission directly from the copyright holder. To view a copy of this licence, visit http://creativecommons.org/licenses/by-nc-nd/4.0/.

© The Author(s) 2024